

Highly resilient, error-protected quantum gates in a solid-state quantum network node

E. Poem, M. I. Cohen, S. Blum, D. Minin, D. Korn, O. Heifler, S. Maayani, A. Hamo, I. Bayn, N. Bar-Gill, M. Tordjman

Quantum Transistors Ltd.,
Hamelacha 6, Binyamina 3057319, Israel
1270 Avenue of the Americas, New York, U.S

Abstract

High-fidelity quantum gates are a cornerstone of any quantum computing and communications architecture. Realizing such control in the presence of realistic errors at the level required for beyond-threshold quantum error correction is a long-standing challenge for all quantum hardware platforms. Here we theoretically develop and experimentally demonstrate error-protected quantum gates in a solid-state quantum network node. Our work combines room-temperature randomized benchmarking with a new class of composite pulses that are simultaneously robust to frequency and amplitude, affecting random and systematic errors. We introduce Power-Unaffected, Doubly-Detuning-Insensitive Gates (PUDDINGs) - a theoretical framework for constructing conditional gates with immunity to both amplitude and frequency errors. For single-qubit and two-qubit CNOT gate demonstrations in a solid-state nitrogen-vacancy (NV) center in diamond, we systematically measure an improvement in the error per gate by up to a factor of 9. By projecting the application of PUDDING to cryogenic temperatures we show a record two-qubit error per gate of 1.2×10^{-5} , corresponding to a fidelity of 99.9988%, far below the thresholds required by surface and color code error correction. These results present viable building blocks for a new class of fault-tolerant quantum networks and represent the first experimental realization of error-protected conditional gates in solid-state systems.

I. INTRODUCTION

A. Background

Fault-tolerant quantum computation requires gate fidelities that exceed stringent error-correction thresholds, typically in the range of 10^{-4} to 10^{-2} for leading quantum error-correcting codes such as surface codes and color codes [1], [2], [3], [4]. Achieving and sustaining such performance in realistic devices is challenging because gate operations must be robust not only to static calibration errors but also to time-dependent noise and drift in both the control fields and the surrounding environment.

Randomized benchmarking (RB) has emerged as the gold standard tool for quantifying the random component of the error per gate (rEPG), which is particularly relevant for fault

tolerance [5], [6], [7], [8], [9], [10], [11]. In RB, one measures the decay of the survival probability under sequences of randomly chosen Clifford operations, allowing gate-dependent stochastic errors to be separated from both state-preparation and measurement (SPAM) errors and the static error per gate (sEPG) [8], [9], [10], [11].

Nitrogen-vacancy (NV) centers in diamond offer unique advantages for distributed quantum networks. The NV center's optical addressability, long coherence times at room temperature, and intrinsic coupling to nearby nuclear spins make it an attractive candidate for quantum communication and distributed quantum computing nodes [12]. Recent RB studies on NV centers have demonstrated promising single-qubit fidelities [13], [14] but conditional two-qubit gates, essential for universal quantum computation and entanglement-based networking, remain limited by sensitivity to spectral diffusion, control-power fluctuations, and dephasing. Therefore, a reliable protected-gate strategy is of imminent importance.

Dynamical decoupling [15], [16], [17], [18], [19] and composite-pulse techniques [20], [21], [22], [23], [24], [25], [26], [27], [28], [29] offer complementary routes to error suppression at the control level. Dynamical decoupling sequences, originally developed in nuclear magnetic resonance, can strongly suppress quasi-static dephasing during idle periods, while composite pulses engineer gate operations from carefully phased sub pulses to cancel systematic amplitude and detuning errors to first or even higher order [21], [30]. Broad-band composite pulses (BB-COMPs) such as BB1 and related families have been successfully applied to single-qubit gates, achieving strong robustness against miscalibrations and inhomogeneities [25], [26], [27], [29]. However, extending these concepts to conditional gates in multilevel, frequency-selective systems introduces additional constraints: one must preserve exact conditional logic (for example, a controlled-NOT gate) while simultaneously protecting both the “active” and “inactive” subspaces from amplitude and detuning noise [30], [31]. Existing approaches to energy-selective conditional gates in such systems either sacrifice speed, suffer from large residual systematic errors, or lack protection against the dominant noise mechanisms. [32]

This gap motivates the development of an adapted and unified framework for error-protected conditional gates that remains compatible with realistic experimental constraints in solid-state devices and, at the same time, is portable to a broad class of physical platforms.

B. Key Contributions

In this work we combine theoretical pulse engineering with room-temperature RB on an NV center platform to introduce and experimentally validate a new class of error-protected conditional gates, which we call Power-Unaffected, Doubly-Detuning-Insensitive Gates (PUDDINGs). Our main contributions are:

1. Comprehensive RB of NV quantum gates. We implement and benchmark the full single-qubit Clifford group for a nuclear-spin qubit and benchmark conditional electron-spin gates, identifying dominant error sources and quantifying their contributions. By decomposing the total rEPGs into components (electron thermalization, electron dephasing, RF power fluctuations), we extract their low-temperature-projected values [33], [34], [35], allowing for direct comparison with the existing methods [32].
2. Introduction of PUDDING: a unified framework for error-protected conditional gates. Building on zero-area pulses, we construct Protected Zero-Area Pulses (P-ZAPs) [36] that implement conditional rotations while being all-orders insensitive to power fluctuations and first-order insensitive to detuning errors on the

inactive subspace. Embedding these P-ZAPs into BB-COMP sequences yields PUDDINGs, which simultaneously achieve (i) exact conditional logic, (ii) at least first-order immunity to both detuning and amplitude errors on both the active and inactive subspaces, and (iii) quadratic scaling of the infidelity with respect to the noise amplitude.

3. Experimental validation and pathway to fault tolerance. Using a single NV center coupled to a nearby ^{15}N nuclear spin, we implement PUDDING-protected single-qubit and two-qubit gates and characterize their performance via randomized benchmarking. For single-qubit nuclear-spin gates at room temperature, PUDDINGs reduce the rEPG by approximately an order of magnitude compared with simple rectangular pulses, despite increasing the gate duration by nearly an order of magnitude. For two-qubit conditional gates, we observe a similar improvement. Combining RB with a microscopic noise model, we then project the performance of PUDDINGs in isotopically purified diamond operated at cryogenic temperatures, where we predict a two-qubit error per gate of 1.2×10^{-5} (99.9988% fidelity), comfortably below surface- and color-code thresholds. These results establish a realistic route to fault-tolerant operations in NV-based quantum network nodes.

C. Significance for Quantum Networks

The NV center platform is particularly well suited for networked and distributed quantum computing, where each node comprises of a small local processor connected to others via photonic entanglement [37]. In this architecture, the electron spin serves as a fast, optically addressable processing qubit, while nearby nuclear spins provide long-lived quantum memory and local register functionality. High-fidelity, noise-robust conditional gates between electron and nuclear spins are therefore a central resource for local entanglement processing, entanglement purification, and error-corrected storage.

Our results demonstrate that error-protected conditional gates can be realized in a solid-state network node even at room temperature, and that realistic improvements in material quality and operating temperature are sufficient to push gate errors significantly below established fault-tolerance thresholds. Because PUDDINGs are constructed solely from phase- and amplitude-shaped pulses acting on a frequency-differentiated two-qubit system, the same design principles can be applied to other qubit architectures in which a control degree of freedom shifts the transition frequency of a target qubit, including superconducting transmons, semiconductor quantum dots, trapped ions, and neutral-atom arrays.

In this sense, our NV-based demonstration serves as a blueprint for a general class of error-resilient conditional gates that do not rely on extensive recalibration or heavy error-correction overhead but instead embed robustness directly at the level of pulse design. This is particularly attractive for modular and networked architectures, where heterogeneous hardware and fluctuating operating conditions can make gate calibration a major bottleneck.

D. Outline

The remainder of the paper is organized as follows. In Sec. II we develop the theoretical framework for error-protected quantum gates. We begin by reviewing error mechanisms in single-qubit rotations and broad-band composite pulses, then introduce zero-area pulses and their augmented, protected counterparts (P-ZAPs), and finally construct the full PUDDING sequences.

Section III describes the experimental NV platform, including the diamond sample, spin structure, control hardware, and the randomized-benchmarking protocols used to quantify rEPG. In Sec. IV we present the experimental results, comparing unprotected and PUDDING-protected single- and two-qubit gates at room temperature and extracting projected performance at low temperature in isotopically purified diamond. Section V discusses the implications of these results for fault-tolerant quantum computation and quantum networking and compares our projected performance to that of other leading platforms. Section VI concludes with an outlook on future applications and extensions of PUDDINGs to other qubit systems. Technical derivations and noise simulations are provided in the Appendices.

II. THEORY OF ERROR-PROTECTED QUANTUM GATES

A. Errors principles in Quantum Operations

Consider a target single-qubit rotation

$$U_{target} = e^{-i\alpha \hat{\mathbf{n}} \cdot \boldsymbol{\sigma}/2},$$

where $\boldsymbol{\sigma} = (\sigma_x, \sigma_y, \sigma_z)$ is a vector of Pauli matrices, α is the rotation angle, and $\hat{\mathbf{n}} = (\cos \theta \cos \phi, \cos \theta \sin \phi, \sin \theta)$ is the rotation axis. Here ϕ is the drive phase, $\tan \theta = \delta/\Omega$, and $\alpha = T\sqrt{\Omega^2 + \delta^2}$, where Ω is the Rabi frequency, proportional to the pulse amplitude, δ is the detuning from resonance, and T is the pulse duration. Typically, resonant driving is used, so $\delta = \theta = 0$, such that

$$U_{target} = e^{-i\alpha[\cos \phi \sigma_x + \sin \phi \sigma_y]/2}.$$

Real pulses suffer from systematic and random errors, $\Omega \rightarrow \Omega(1 + \epsilon(t))$, and $\delta(t) = \Omega\eta(t) \neq 0$. In many cases, timing and phase errors can be neglected with respect to amplitude and detuning errors. In this case, and for small errors, $\epsilon(t), \eta(t) \ll 1$, the actual propagator becomes:

$$U_{actual} \approx e^{-i\alpha[\cos \phi \sigma_x + \sin \phi \sigma_y]/2 - i\Omega \int_0^T dt [\epsilon(t)(\cos \phi \sigma_x + \sin \phi \sigma_y) + \eta(t)\sigma_z]/2}.$$

The error per gate (EPG) can then be quantified by using the Frobenius distance of U_{actual} from U_{target} . This is just the square root of the mean of the squares of the differences between the elements of the matrices. For systematic errors, as well as for quasi-static noise, that is, when the noise is approximately constant over the pulse duration, one obtains to the lowest order in the noise magnitudes,

$$EPG = \frac{1}{\sqrt{2}} \left| \sin \frac{\alpha}{2} \right| \sqrt{\eta^2 + \epsilon^2}.$$

We see that even in this case of quasi-static noise, the EPG is linear in the combined magnitude of the pulse amplitude (ϵ) and frequency (η) noise. For example, for quasi-static frequency noise, defined by $\Omega\eta = 1/T_2^*$, where T_2^* is known as the inhomogeneous dephasing time, the EPG would scale as $1/\Omega T_2^*$. As the gate duration, T_g , scales as $T_g \propto 1/\Omega$, the EPG due to quasi-static frequency noise would scale as T_g/T_2^* . A similar relation holds also for quasi-static amplitude noise.

Dynamical decoupling [38], [39] can suppress dephasing during idle periods by periodically flipping the qubit phase, but it cannot protect the quantum state during gate operation where the desired rotation must

occur. Composite pulses address this by constructing the target operation from sub-pulses with carefully chosen phases and amplitudes such that error terms cancel to first (or higher) order.

Figure 1 summarizes, at a qualitative level, the protection offered by unprotected single- and two-qubit gates, dynamical decoupling protocols (CPMG [15] [16] [18], XY8 [40], [41], [42], [43], AXY [19], [44]), and the PUDDING gates introduced in this work. For each, we indicate whether single- and two-qubit operations are protected or vulnerable to pulse-frequency (detuning) noise and pulse-power (amplitude) noise. PUDDING gates are the only strategy that achieves full single- and two-qubit logic while protecting against both amplitude and detuning noise. More detailed information is presented in Appendix I.

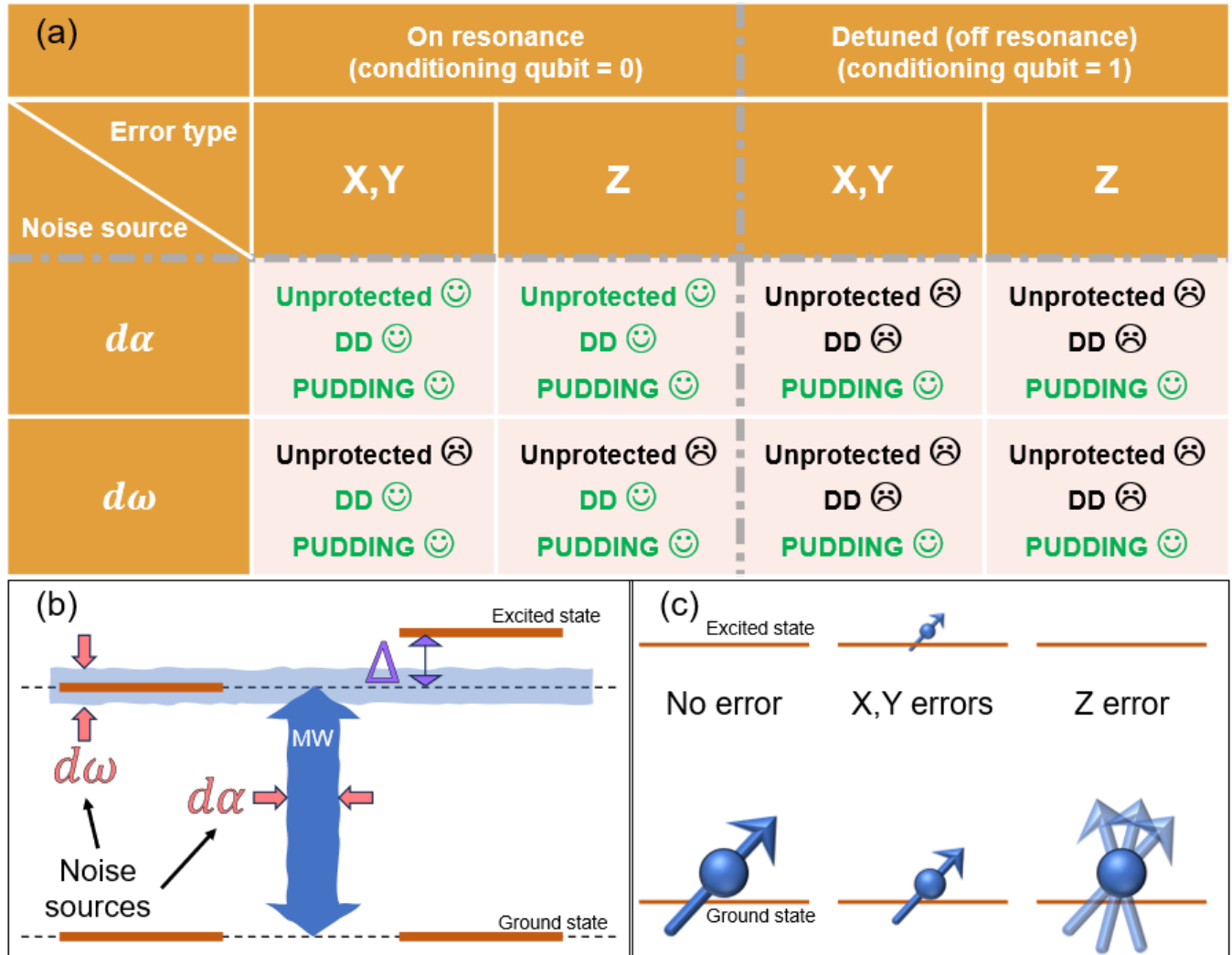


Figure 1: Noise sources and error types. (a) The ability of different gate protocols to handle errors from different noise channels. Unprotected gates relate to simple ZAPs (see text). DD protocols are sequences based on Dynamical Decoupling (e.g. XY8 [40], [41], [42], [43], AXY [19] [44], etc.). PUDDING protocol is the main protocol discussed in this work. (b) Noise sources – $d\alpha$ is pulse amplitude (Rabi frequency) noise and $d\omega$ is resonance frequency noise. (c) Error types – X,Y are bit-flip errors (over/under rotations), and Z errors are phase flip errors.

B. Broad-Band Composite Pulses (BB-COMPs)

Broad-band composite pulses (BB-COMPs) [21], [45], [28], [46], [26] compensate systematic errors and quasi-static noise by nullifying derivatives of the fidelity with respect to error parameters. A composite π pulse comprises of N simple π pulses with phases $\{\phi_k\}$:

$$U_{\pi,comp} = \prod_{k=1}^N U(\pi, \phi_k),$$

where $U(\pi, \phi_k) = e^{-i\pi[\cos \phi_k \sigma_x + \sin \phi_k \sigma_y]/2}$. For a sequence of three π pulses with phases of $\{0, \phi, 0\}$, choosing $\phi = \pi/2$ nullifies the first-order amplitude derivative of the EPG, $\frac{\partial EPG}{\partial \epsilon} \Big|_{\epsilon=0} = 0$. However, three pulses of equal rotation angle cannot simultaneously zero both $\frac{\partial EPG}{\partial \epsilon}$ and $\frac{\partial EPG}{\partial \eta}$.

Five-pulse sequences with optimized phases achieve such dual protection. The U5a sequence [47], [46], [26] employs five π pulses with phases of $\{0, 5\pi/6, \pi/3, 5\pi/6, 0\}$, achieving $\frac{\partial EPG}{\partial \epsilon} = \frac{\partial EPG}{\partial \eta} = 0$ with a total duration $T_{U5a} = 5\pi/\Omega$.

Such composite pulses share the property that second-order derivatives are non-zero, and thus residual errors scale as $O(\epsilon^2, \eta^2, \epsilon\eta)$. This quadratic scaling means that for a given inhomogeneous dephasing time T_2^* , the error in a gate of length T_g scales as $(T_g/T_2^*)^2$ instead of T_g/T_2^* as for simple, unprotected gates. This is the reason why composite pulses may provide an advantage even though they may be considerably longer than simple pulses.

Protected composite pulses that rotate by angles other than π are known [24], but with protection only against amplitude errors. To include protection also against detuning errors for any desired rotation angle, α , we considered a seven-pulse sequence made of five π pulses sandwiched between two $(\pi - \alpha)/2$ pulses, and found (Appendix II) the required phases to be $\{0, g(\alpha), 2g(\alpha) + h(\alpha), 2g(\alpha) + 2h(\alpha), 2g(\alpha) + h(\alpha), g(\alpha), 0\}$. Here $g(\alpha) = \cos^{-1}(-\alpha/4\pi - 1/4 \cdot \sin \alpha/2)$, and $h(\alpha) = \cos^{-1}(-\alpha/4\pi + 1/4 \cdot \sin \alpha/2)$. For $\alpha = \pi$ this sequence reduces to U5a.

C. Energy-Selective Conditional Gates (ES-CONGs)

Consider a two-qubit system with states $\{|00\rangle, |01\rangle, |10\rangle, |11\rangle\}$ where qubit 1 (control) modulates qubit 2's (target) transition frequency by Δ :

$$\omega_2^{(0)} = \omega_0, \quad \omega_2^{(1)} = \omega_0 + \Delta.$$

The goal is to flip qubit 2 conditionally: $|m_1 m_2\rangle \rightarrow |m_1 \bar{m}_2\rangle$ only for $m_1 = 1$, while for $m_1 = 0$ leaving the second qubit unchanged. There are several known ways of achieving this goal.

1. Weak-Interaction Regime ($\Omega \ll \Delta$): Tune a resonant pulse to $\omega_0 + \Delta$. Off-resonant excitation of the ω_0 transition is then suppressed. However, it is never exactly zero, even without any noise, always leaving a residual gate infidelity of $|\Omega/\Delta|$. As the required gate time is π/Ω , decreasing the infidelity requires increasing the pulse duration, eventually running into the inhomogeneous dephasing time, T_2^* . This limits the minimal gate error to $\sim \pi/\Delta T_2^*$.

2. Strong-Interaction Regime ($\Omega \gg \Delta$): Apply two pulses of duration $\tau_p = \pi/2\Omega$ and center frequency $\omega_0 + \Delta/2$, phase-shifted by $\pi/2$ and separated by $T_{sep} = \pi/\Delta$. The differential light shift induces a π rotation for the $\omega_0 + \Delta$ transition while the ω_0 transition acquires only a phase. The residual error, even without noise, scales as $|\Delta/\Omega|$, requiring large Ω to keep suppress this effect.

3. $\pi - 2\pi$ Gate ($\Omega \sim \Delta$): This is an exact conditional gate. It applies a single pulse, resonant with $\omega_0 + \Delta$, choosing $\Omega = \Delta/\sqrt{3}$ and $T = \sqrt{3}\pi/\Delta$. This choice ensures that the resonant transition undergoes a π rotation, while the detuned transition experiences a 2π rotation, returning to its initial state. While exact, this gate is still first-order sensitive to both ϵ and η for both transitions.

Gap in prior work: None of these approaches protect either of the inactive (unity operation) or the active (flip operation) subspace against systematic or random errors. This motivates our development of P-ZAPs and PUDDINGs.

D. Zero-area pulses and P-ZAPs

A zero-area pulse (ZAP) satisfies the condition $\int_{-\infty}^{\infty} \Omega(t) dt = 0$. The simplest ZAP consists of two rectangular pulses of equal amplitude and duration but opposite phase (coinciding with a Walsh-1 wavelet). For a resonant two-level system, the first pulse rotates the Bloch vector away from the north pole and the second pulse reverses this rotation, yielding a net identity operation. Any constant amplitude error scales both halves equally, preserving the zero net area and hence the identity to all orders in the amplitude error.

For a detuned transition with detuning $\delta = \Delta$, choosing $\Omega = \Delta$ and $T = \pi/\sqrt{2}\Delta$ leads to a net π rotation of the detuned transition while leaving the resonant transition as identity. Thus, the ZAP acts as a simple conditional gate: identity on resonance and a π flip at detuning of Δ from resonance. However, it remains first-order sensitive to detuning errors on the resonant transition and to both detuning and amplitude errors on the detuned transition. Figure 2(a) presents this pulse and its effects on the Bloch spheres of the on-resonance and detuned subspaces. Residual first-order errors remain in all the component of the over-all rotation.

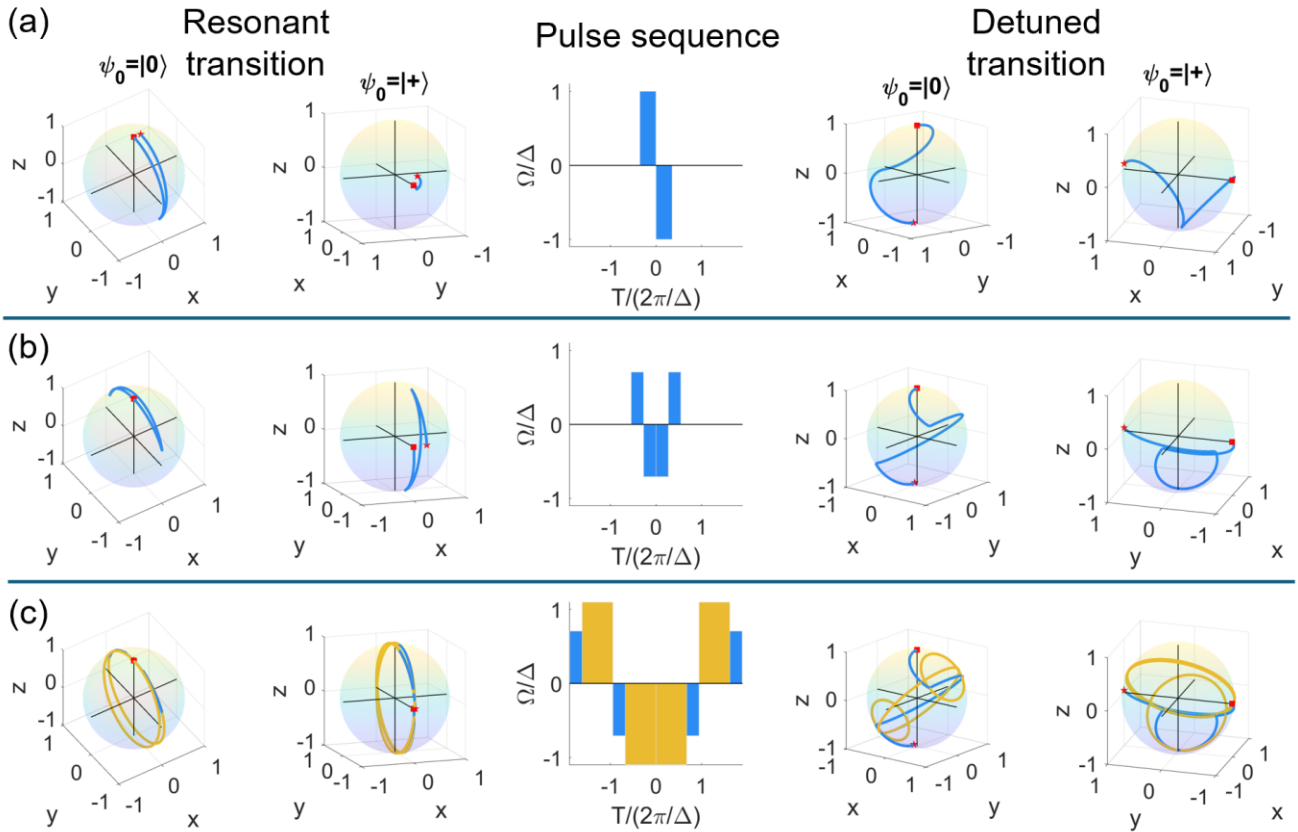


Figure 2: Zero-area conditional gate pulse sequences. (a) The simple Walsh-1 ZAP gate. (b) The symmetric (Walsh-3) ZAP gate. (c) The protected ZAP (P-ZAP) gate (Eq. (1), $p = +1$). In each row, the middle panel presents the Rabi frequency profile, and the left (right) two panels present Bloch sphere trajectories for the on-resonance (Δ detuned) transition for two different initial states (red squares), for a detuning error of 0.05Δ . The final states are marked by red stars. The augmenting pulses of the P-ZAP are colored yellow. One can see that for the on-resonance transition, the P-ZAP (c) gate is the only one that compensates for the detuning error for both initial states.

To suppress first-order detuning errors on the resonant transition, we construct time-symmetric ZAPs. Using the Magnus expansion, one can show (Appendix III) that if a ZAP is symmetric (ABBA structure with A and B equal-amplitude pulses of opposite phases, coinciding with a Walsh-3 wavelet), the first order σ_x and σ_y error terms vanish. For a π rotation on the detuned transition we find (Appendix IV) that the Walsh-3 sequence has to have:

$$\Omega_A = -\Omega_B = \Delta/\sqrt{2}, \quad \alpha_A = \alpha_B = \frac{2\pi}{3\sqrt{3}}$$

Figure 2(b) presents this pulse and its effects on the Bloch spheres of the on-resonance and detuned subspaces. Residual first-order errors remain in the σ_z component.

Complete first-order protection requires augmentation of the symmetric ZAP with compensating pulses. Consider the sequence ACBDDBCA, where A, B are the original opposite-sign rotations and C, D are

augmenting pulses designed to cancel the on-resonance σ_z error of A, B respectively. To keep the total area at 0, the combined area of C and D has to be 0. Further, for them not to affect the detuned-transition action of the original pulses, the augmenting pulses are required to be 2π -pulses on that transition.

There are two mutually exclusive conditions (Appendix III) for first-order σ_z cancellation:

Condition 1 (tangent relation):

$$|\Omega_c| \tan \frac{\alpha_A}{2} = -|\Omega_a| \tan \frac{\alpha_C}{2}$$

Condition 2 (cosine relation):

$$\cos \frac{\alpha_A + p\alpha_C}{2} = 0, \quad p = \pm 1$$

Using Condition 1 together with the zero-area and 2π requirements, this yields:

$$\Omega_c = -\Omega_d = \pm 1.0969 \Delta, \quad \alpha_c = \alpha_d = 1.478\pi$$

with total duration:

$$T_{P-ZAP} = 4(\alpha_A/|\Omega_A| + \alpha_C/|\Omega_C|) \approx 3.784 \times (2\pi/\Delta)$$

The P-ZAP achieves $\partial EPG/\partial \epsilon = 0$ to all orders and $\partial EPG/\partial \delta = 0$ to first order for the resonant (inactive) transition, while performing an exact π rotation on the detuned (active) transition. Its structure and effect on the Bloch spheres are shown in Figure 2(c). Detuning and power errors on the active transition still contribute at first order, motivating the final construction.

E. PUDDINGs: Complete Error Protection for Conditional Gates

To protect both transitions against both detuning and power errors, we embed P-ZAPs into BB-COMP frameworks, yielding Power-Unaffected, Doubly-Detuning-Insensitive Gates (PUDDINGs).

Construction: Replace each π pulse in a BB-COMP (e.g., U5a) with a P-ZAP, adjusting the overall phase of each P-ZAP according to the BB-COMP prescription. For U5a, this yields:

$$U_{PUDDING-U5a} = \prod_{k=1}^5 e^{-i\phi_k \sigma_z/2} U_{P-ZAP} e^{i\phi_k \sigma_z/2}$$

where $\{\phi_k\}_{k=1}^5 = \{0, 5\pi/6, \pi/3, 5\pi/6, 0\}$, and U_{P-ZAP} is the P-ZAP transformation matrix.

Error Suppression: The resulting PUDDING inherits:

- All-orders power insensitivity on the resonant (no-action) transition from the ZAP structure.
- First-order detuning insensitivity on the resonant transition from P-ZAP augmentation.
- First-order power and detuning insensitivity on the detuned (action) transition from the BB-COMP framework.

Figure 3 compares the Frobenius-distance infidelity of a simple Walsh-1 ZAP and a U5a PUDDING gate as functions of detuning and amplitude errors, for both the resonant and detuned subspaces. The narrow valley of low error surrounding the ideal operating point is dramatically broader and more isotropic for PUDDING, clearly demonstrating quadratic error suppression in both control parameters.

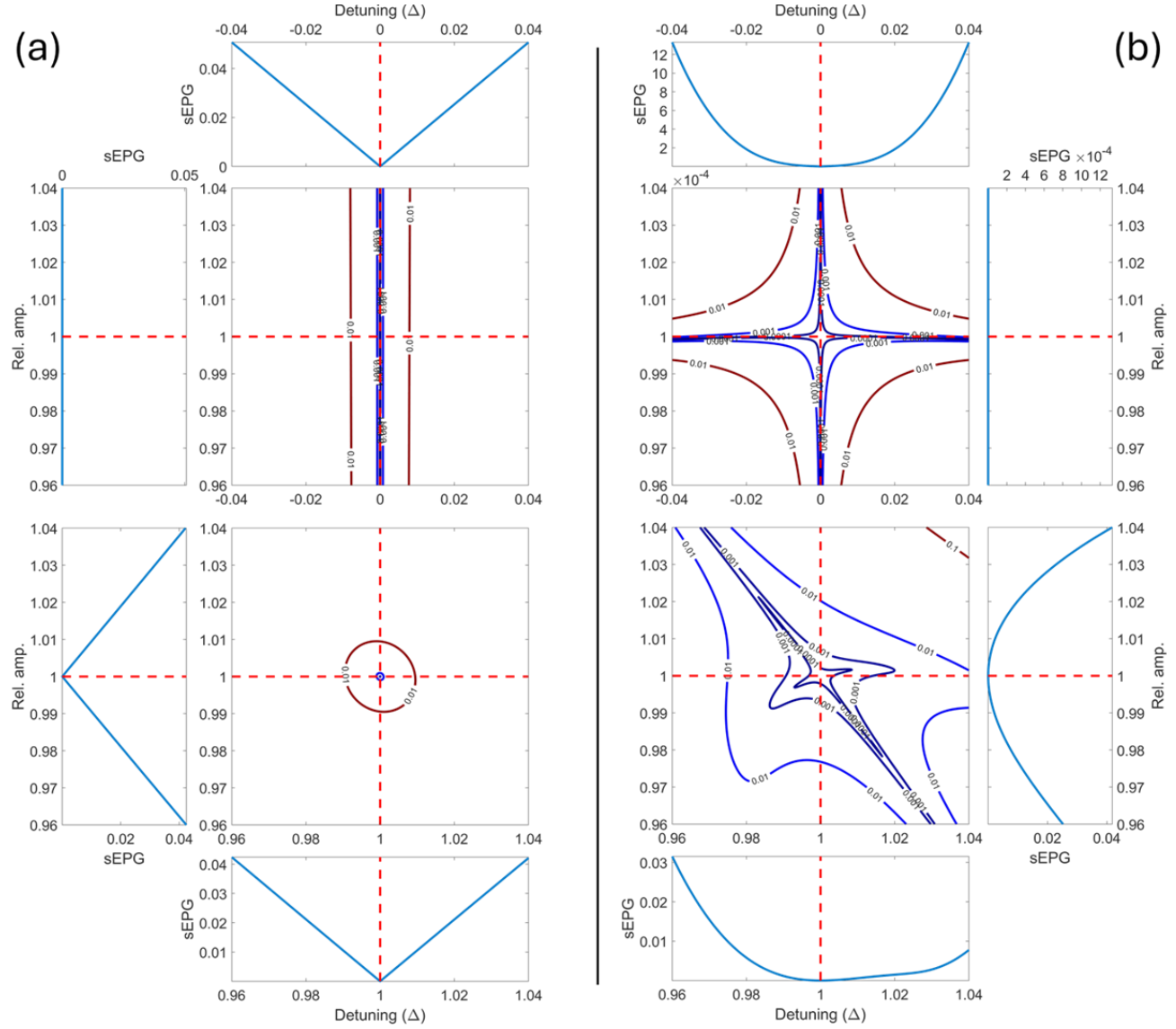


Figure 3: Gate infidelity versus detuning and amplitude. (a) Walsh-1 ZAP. (b) PUDDING U5a (Eq. (1), $p = +1$). For each gate, the top (bottom) panel shows the infidelity with respect to the unit operation, I , (a π rotation about an equatorial axis) around the (off-) resonant transition. The side panels show cuts of the fidelity along the dashed red lines in the main panels.

F. Effect of dephasing and amplitude noise

We now incorporate dephasing into our analysis. Inhomogeneous dephasing is captured by a quasi-static detuning distribution characterized by T_2^* , while homogeneous dephasing (finite T_2) is modeled by a time-dependent stochastic detuning with a specified power spectrum (appendix V). For each noise realization we compute the gate propagator numerically and extract the fidelity relative to the ideal transformation.

Figures 4 and 5 show the total infidelity for representative single- and two-qubit gates, respectively, as a function of T_2^* . Figure 5 also includes curves for several finite values of T_2 . As expected, unprotected gates display large infidelities when T_2^* is shorter than the gate duration, with their errors decreasing roughly as $1/T_2^*$ for longer T_2^* . In contrast, PUDDING gates remain accurate even when T_2^* is almost an order of magnitude shorter than their (longer) durations, and in the regime where T_2^* exceeds all gate durations the PUDDING infidelity decreases approximately as $1/(T_2^*)^2$, reflecting the first-order detuning insensitivity of the composite design.

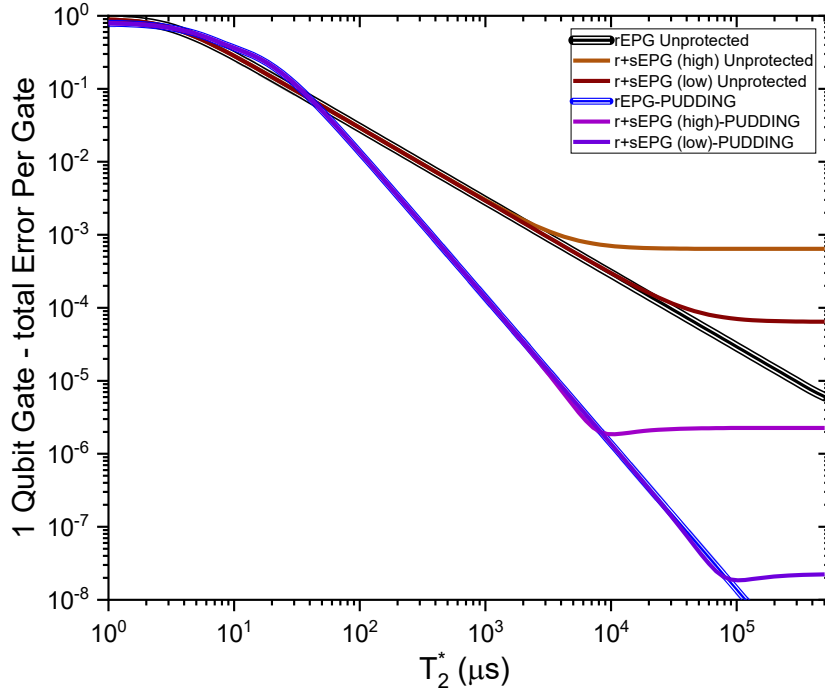


Figure 4: Single-qubit gate fidelity versus the inhomogeneous dephasing time for unprotected and PUDDING protected protocols. The solid lines assume infinite homogeneous dephasing time. The black (blue) lines present the average random error per gate (rEPG) of unprotected (PUDDING) Clifford gates, calculated for quasi-static spectral noise with a Gaussian spectral width of $1/T_2^*$. The Rabi π time of a simple pulse is set to $13 \mu\text{s}$, as in our experiment. The mean gate time is then $6.5 \mu\text{s}$ ($58.5 \mu\text{s}$) for the unprotected (PUDDING) gates. The brown and light brown (purple and light purple) lines present the total EPG (rEPG+sEPG) for the unprotected (PUDDING) gates, now including a systematic relative amplitude error per gate (sEPG) respectively.

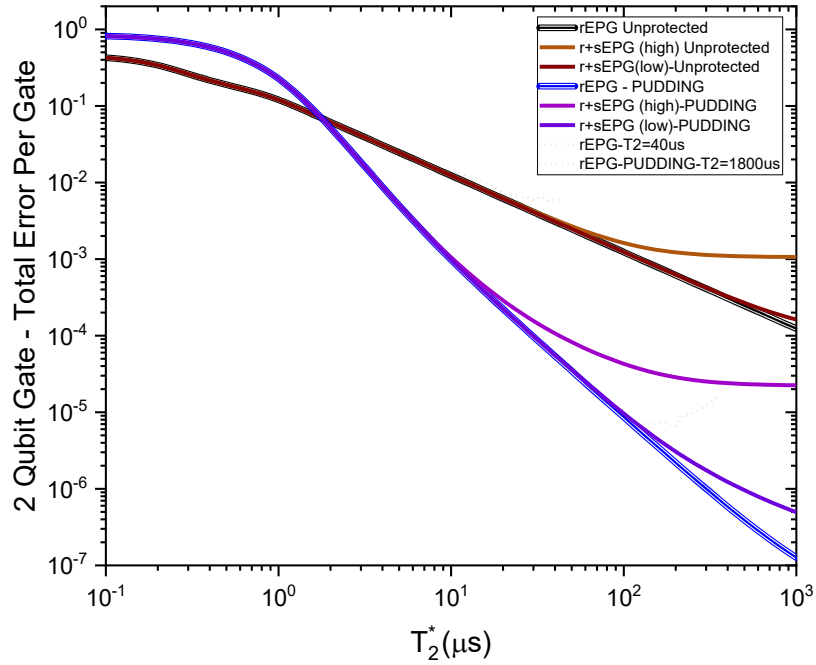


Figure 5: Two qubit gate fidelity versus the inhomogeneous dephasing time for unprotected and PUDDING protected protocols. The solid lines assume infinite homogeneous dephasing time. The broken lines include finite homogeneous dephasing time, as labeled. The black (blue) shaded lines present the average random error per gate (rEPG) of unprotected (PUDDING) CNOT gates, calculated for quasi-static spectral noise with a Gaussian spectral width of $1/T_2^*$. The unprotected (PUDDING) gate time is $0.234 \mu\text{s}$ ($6.24 \mu\text{s}$). The brown and light brown (purple and light purple) lines present the total EPG (rEPG+sEPG) for the unprotected (PUDDING) gates, now including a systematic relative amplitude error per gate (sEPG), respectively. The dotted lines present the rEPG including dynamical noise, characterized by T_2 of $40 \mu\text{s}$ ($1800 \mu\text{s}$) for the unprotected (PUDDING) gate.

Finite homogeneous dephasing imposes a floor on achievable fidelity, reached for sufficiently large T_2^* . This floor is more severe for longer gates and eventually limits the performance of the longest PUDDING sequences. Nevertheless, for a broad range of parameters relevant to NV centers, PUDDING gates still outperform simpler gates by a substantial margin, even when homogeneous dephasing is included.

III. EXPERIMENTAL PLATFORM AND METHODS

A. Diamond Sample and NV Centers

Our experiments employ a 20-μm-thick (001) diamond membrane implanted with ^{15}N ions at a density optimized for single-NV isolation. Following implantation at 30 keV and annealing at 800°C for 2 hours, NV centers formed approximately 30 nm below the surface. Confocal fluorescence microscopy and Hanbury Brown-Twiss intensity correlation measurements ($g^{(2)}(0) < 0.5$) confirmed the location of single NVs. The

overall photon collection efficiency, including objective numerical aperture (NA = 0.9), optical transmission, and avalanche photodiode (APD) quantum efficiency, reached 8.6%, enabling high signal-to-noise ratio.

B. Spin Structure and Control

The NV center's electronic ground state is a spin-1 triplet ($m_s = 0, \pm 1$), split by ~ 2.87 GHz at zero field. A permanent magnet (~ 10 mT) oriented along the NV axis further splits the $m_s = \pm 1$ states by ~ 560 MHz, isolating $\{|m_s = 0\rangle, |m_s = +1\rangle\}$ as a well-defined qubit. The ^{15}N nuclear spin ($I = 1/2$) experiences a hyperfine and Zeeman splitting of 2.98 MHz when $m_s = +1$ and 0.05 MHz when $m_s = 0$. This large frequency difference enables selective nuclear spin manipulation conditioned on the electron state, and vice versa.

C. Control Apparatus

Microwave (MW) control: Electron spin rotations employ resonant MW pulses at ~ 2.55 GHz, delivered via a printed circuit-board (PCB) loop antenna placed ~ 50 μm beneath the sample. Rabi frequencies $\Omega_e/2\pi \approx 5 - 10$ MHz enable π pulses in $\sim 50 - 100$ ns.

Radiofrequency (RF) control: Nuclear spin rotations utilize RF pulses at ~ 3 MHz, delivered through the same antenna. Rabi frequencies $\Omega_n/2\pi \approx 40$ kHz yield π pulse durations of ~ 13 μs . Power stability of the RF amplifier (specified at $\pm 0.5\%$) and frequency stability (± 10 Hz) set fundamental limits on ϵ and η .

Optical initialization and readout: A 520-nm laser (140 μW , 700 ns pulse) spin-polarizes the electron to $|m_s = 0\rangle$ with $>90\%$ efficiency via optical pumping. Fluorescence under 520-nm excitation distinguishes $m_s = 0$ (bright) from $m_s = +1$ (dark) with a contrast of $\sim 30\%$, enabling high-fidelity readout.

D. Single-Qubit Gate Construction

A "pure" nuclear spin gate (electron spectator) requires compensation for the electron's state-dependent hyperfine shift. We employ a double-passage protocol:

1. Apply RF pulse at $\omega_n^{(1)}$ (electron in $| + 1\rangle$).
2. Flip electron: MW π pulse $| + 1\rangle \rightarrow | 0\rangle$.
3. Apply RF pulse at $\omega_n^{(1)}$ again.
4. Flip electron back: MW π pulse $| 0\rangle \rightarrow | + 1\rangle$.

Since MW pulses (~ 50 ns) are $\sim 100\times$ faster than RF pulses (~ 6.5 μs on average), their contribution to gate error is negligible, and the effective single-qubit gate error is dominated by RF pulse imperfections.

E. Two-Qubit Conditional Gate (C_nNOT_e)

We implement a controlled-NOT with the nuclear spin as control and electron as target (C_nNOT_e) using a zero-area pulse sequence:

1. Apply two consecutive MW pulses resonant with $| m_s = 0, m_I = -1/2\rangle \leftrightarrow | m_s = +1, m_I = -1/2\rangle$.
2. Each pulse has a duration of $\pi/\sqrt{2}\Delta$, where $\Delta \approx 3$ MHz is the MW transition energy difference between states of $m_I = -1/2$ and $m_I = 1/2$.
3. Set the Rabi frequency to Δ and the relative phase between the two pulses to π .

For $m_l = -1/2$ (resonant), the net rotation is identity (zero area). For $m_l = +1/2$ (detuned by hyperfine), the electron executes a π flip. This gate is exact but first-order sensitive; we later test composite versions.

F. Randomized Benchmarking Protocol

For single-qubit gates, we implement the full 24-element Clifford group C_1 using decompositions into $\{X_{\frac{\pi}{2}}, Y_{\frac{\pi}{2}}, Z_{\frac{\pi}{2}}\}$. Each Clifford is compiled into a sequence of 1-3 RF pulses with appropriate phases.

For sequence length m :

1. Initialization: Optical pump + MW conditioning $\rightarrow |m_s = +1, m_l = +1/2\rangle$.
2. Random Clifford sequence: Apply m Clifford gates $\{C_1, C_2, \dots, C_m\}$ drawn uniformly from the Clifford group.
Inversion: Apply $C_{inv} = (C_m \dots C_2 C_1)^{-1}$.
3. Readout: Measure return probability $P_{return}(m)$.

We apply $N_{trials} > 10^4$ random sequences per m , averaging to extract $\langle P_{return}(m) \rangle$.

The return probability decays exponentially:

$$\langle P_{return}(m) \rangle = A p^m + B$$

where p is the average Clifford survival probability and A and B account for SPAM errors. The random error per gate (rEPG) is:

$$rEPG = (d - 1)/d \times (1 - p)$$

with $d = 2$ for a single-qubit gate. Statistical uncertainties are propagated from the fit covariance matrix.

To isolate gate errors from electron relaxation, we perform a reference RB where the RF gates are replaced by idle periods of equal duration. The difference between full RB and reference RB decay rates isolates the RF gate error contribution.

IV. EXPERIMENTAL RESULTS

A. Single-qubit unprotected gates: simple RF pulses

We first benchmark nuclear single-qubit gates implemented by simple rectangular RF pulses with average duration of about 6.5 μ s. Randomized benchmarking yields a total rEPG on the order of 3×10^{-3} , as presented in Figure 6(upper) by the blue symbols and line. Reference RB sequences with identical timing but without RF pulses reveal that a substantial fraction of this error arises from electron T_1 relaxation during the RF gate, as presented by the red symbols and line in Figure 6 (upper). The remaining error is attributed to RF power fluctuations, nuclear dephasing, and residual crosstalk.

Independent estimates from RF amplifier stability and Ramsey measurements indicate quasi-static amplitude and detuning noise at the 0.1–0.2% level and nuclear spin T_2^* of a few milliseconds, which together

account for errors of a few 10^{-4} – 10^{-3} per gate. These unprotected gates set the baseline performance against which composite protocols are compared.

B. Single-qubit PUDDING-protected gates

We next replace each simple RF pulse with an appropriate PUDDING composite sequence: a five-pulse U5a structure for π rotations and a seven-pulse generalization for arbitrary angles. The average gate duration increases by a factor of about nine.

Despite this increase, as can be seen in Figure 6 (lower), randomized benchmarking reveals a substantial improvement: after subtracting the electron-relaxation contribution obtained from reference RB, we obtain a single-qubit PUDDING rEPG of about 1.9×10^{-4} in our natural-abundance diamond sample at room temperature, compared with 2.9×10^{-3} for simple pulses. Thus, PUDDINGs reduce the nuclear gate error by roughly an order of magnitude, even though the gates are significantly longer.

Using our noise model and measured coherence times, we project that in isotopically purified ^{12}C diamond at cryogenic temperatures, single-qubit PUDDING gates achieve rEPG values as low as 2×10^{-7} , even in the presence of realistic amplitude fluctuations at the 0.1–1% level. These projected error rates are well below standard surface- and color-code thresholds.

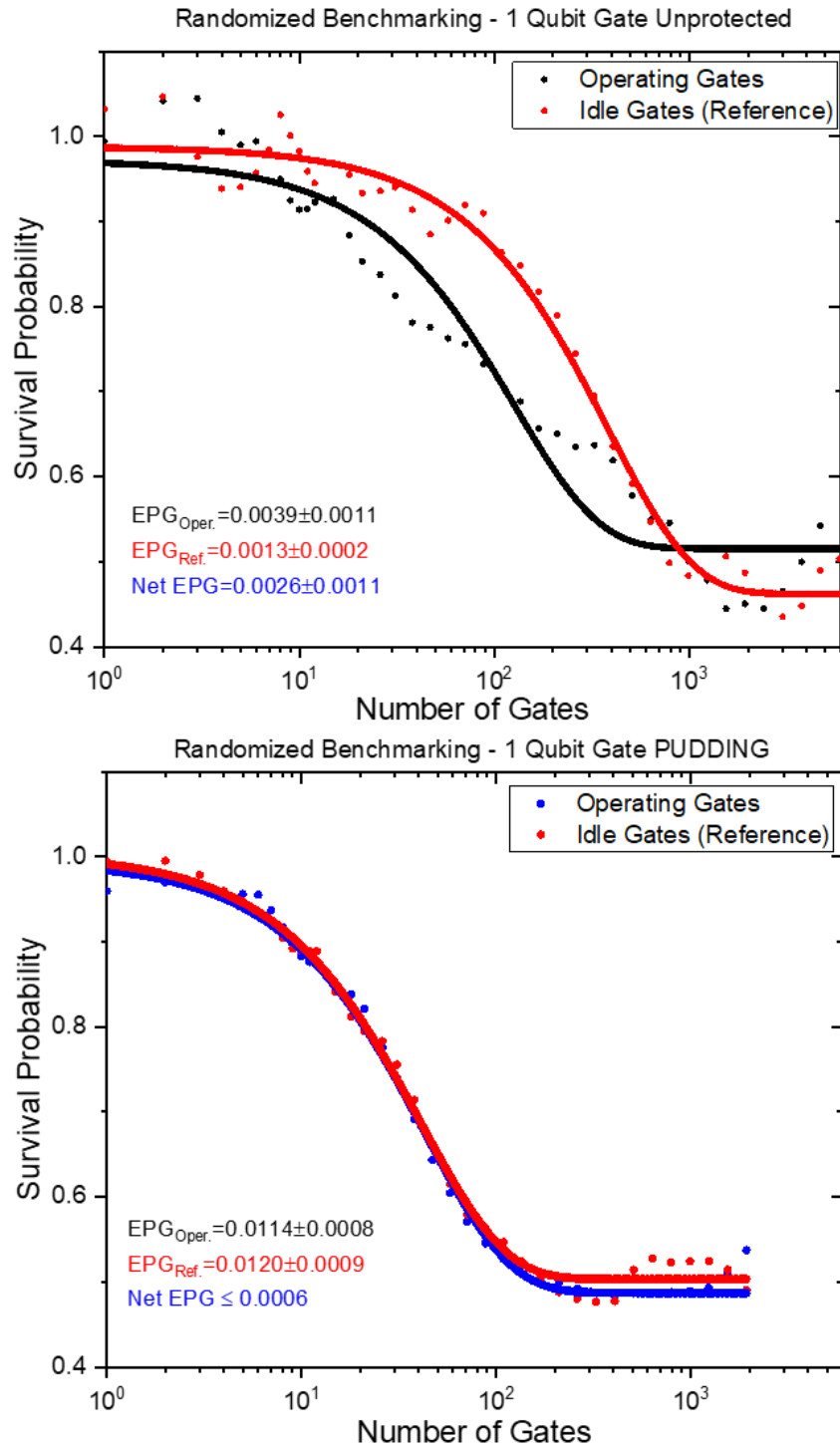


Figure 6 – Randomized benchmarking of single-qubit gates. The measured single-qubit gates data (fit) are presented by dots (line). Respective reference data (fit) are presented by the red dot (dotted line). For reference data, the same initialization and measure protocols were used, where instead of applying the gates, the system was kept idle for the same duration as that of the gates (Idle Gates). (Upper) Unprotected gates in black. (Lower) PUDDING Protected gates in blue.

The data is fitted to $P(N) = Ae^{-B \cdot N} + C$, extracting the average error per gate as $EPG = \frac{1-e^{-B}}{2}$. allowing us to ignore SPAM infidelity and searching only for B.

The measured data (fit) are presented by the blue down-pointing triangles (solid line), while the reference data (fit) are presented by the red up-pointing triangles (dotted line).

For the reference data, the same initialization and measure protocols were used, where instead of applying the gates, the system was kept idle for the same duration as that of the gates.

(a) unprotected gates – The X gates are performed by applying a constant RF field for durations that fit the desired rotation (π is approx. 13 μ s).

Gates EPG is given by 0.0039 ± 0.0011 . The reference EPG is 0.0013 ± 0.0002 , and the net EPG is given by their subtraction from each other, with the confidence bounds summed independently (square root of sum of squares) yielding 0.0026 ± 0.0011 .

(b) protected gates – The X gates are performed by applying a set of RF pulses with phase jumps according to the main text.

Gates EPG is 0.0114 ± 0.0008 . The reference EPG is 0.0120 ± 0.0009 . If the net EPG was taken by their subtraction from each other, it will be negative, but with a value smaller than the confidence bounds, resulting in net EPG which is limited by $-0.0006 \pm 0.0012 \leq 0.0006$.

In both (a) & (b) the reference EPG corresponds to the ratio between the gate duration T_{gate} and the electron T_1 . This explains why although it seems that our protocol has worsened our gate EPG (as the gate durations increased), those results offer the prospect that for a system with longer T_{1e} (e.g. at 4°K, $T_{1e} \gg 10$ s), the effective EPG will become diminishingly low.

C. Two-qubit conditional unprotected gates: simple zero-area pulses

For two-qubit conditional gates we first benchmark the simple zero-area MW sequence implementing $C_n NOT_e$. Each MW pulse has duration $\tau \approx 117$ ns, for a total gate time of about 234 ns. We estimate the gate error using an interleaved RB-style protocol in which we repeatedly apply the $C_n NOT_e$ gate m times followed by its inverse applied m times and measure the survival probability of an initially flipped state as a function of m . The results are presented in Figure 7 (upper).

The extracted rEPG for the unprotected zero-area gate is on the order of 3.7×10^{-2} , dominated by electron inhomogeneous dephasing with $T_2^* \approx 3 \mu$ s in natural-abundance diamond. Simple estimates based on T_2^* and gate duration reproduce this value, and the result is largely unaffected by adding amplitude noise at the 1% level, as frequency and amplitude errors add in quadrature.

D. Two-qubit PUDDING-protected gates

We then construct P-ZAP-based conditional gates using the ACBDDBCA sequence and embed these P-ZAPs into a U5a composite structure to obtain a two-qubit PUDDING gate. This increases the total gate duration by a factor of roughly 27 compared to the simple zero-area gate.

As shown in Figure 7 (lower), benchmarking via the same repeated-gate protocol yields a two-qubit PUDDING EPG of about 4.0×10^{-3} in the natural-abundance sample at room temperature. Compared to the value of 3.7×10^{-2} for the unprotected gate, this is an improvement by a factor of about 9, achieved despite the 27-fold increase in gate duration, underscoring the power of error cancellation at the pulse-design level.

When projected to isotopically enriched ^{12}C diamond at 4 K using experimentally informed noise models, the PUDDING protocol approaches or surpasses the two-qubit error levels reported in other leading platforms, while retaining the distinctive advantages of NV centers for modular and distributed architectures.

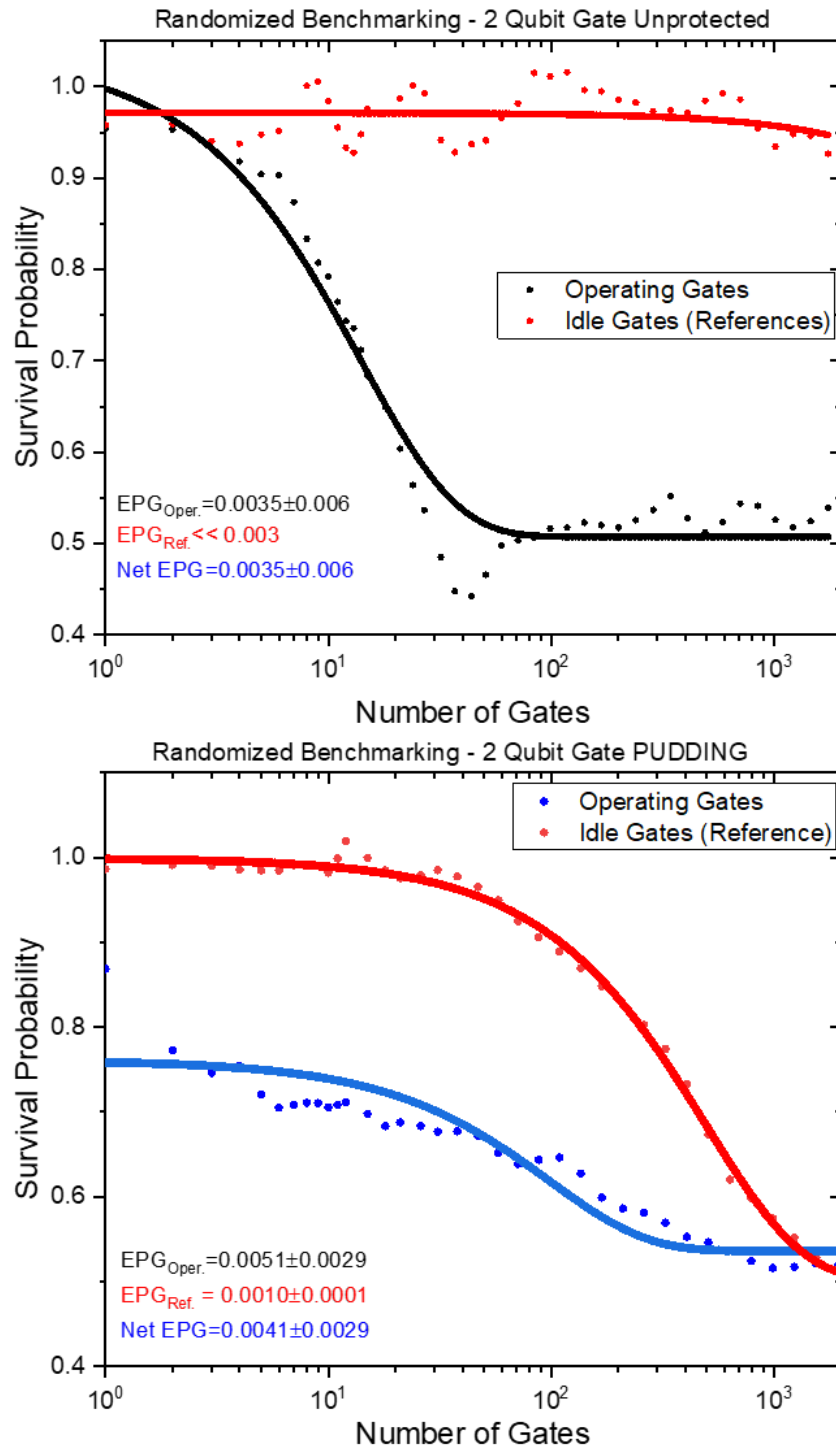


Figure 7 – Benchmarking of a two-qubit gate. The measured two-qubit gates data (fit) are presented by the dots (line). Respective reference data (fit) are presented by the red dot (red line). For the reference data, the same initialization and measure protocols were used, where instead of applying the gates, the system was kept idle for the same duration as that of the gates. (Upper) Unprotected gates in black . (Lower) PUDDING Protected gates in blue.

E. Projection to isotopically purified diamond

Isotopic enrichment to >99.9% ^{12}C extends electron T_2^* from about 3 μs to approximately 250 μs and Hahn-echo T_2 from about 40 μs to nearly 1.8 ms. At 4K, electron T_1 exceeds 1 s, effectively removing T_1 as a limiting factor on gate fidelity. Under these conditions, our noise model predicts that two-qubit PUDDING gates achieve an error per gate of 1.2×10^{-5} , while unprotected gates remain at the level of a few 10^{-4} .

Including amplitude noise at the 0.1–1% level increases the PUDDING error only marginally, to a few 10^{-5} . These values are roughly 400 \times below a typical surface-code threshold and about 100 \times below a representative color-code threshold, demonstrating a realistic path to fault-tolerant, error-protected conditional gates in NV-based quantum network nodes. Table 2 summarizes all measured and projected EPGs and gate durations for both single- and two-qubit gates in natural abundance and isotopically purified samples at room temperature and 4 K.

Quantum Gates :	1 Qubit Gate				2 Qubit Gate			
Protocol Application 4K	Unprotected		PUDDING		Unprotected		PUDDING	
Sample purity grade	ELSC	C^{12}	ELSC	C^{12}	ELSC	C^{12}	ELSC	C^{12}
Error Per Gate	2.93×10^{-3}	1.9×10^{-4}	3.2×10^{-4}	2×10^{-7}	3.7×10^{-2}	4×10^{-4}	4.5×10^{-3}	1.2×10^{-5}
Gate Time (sec)	6.5×10^{-6}	6.5×10^{-6}	5.8×10^{-5}	5.8×10^{-5}	2.32×10^{-7}	2.32×10^{-7}	6.24×10^{-6}	6.24×10^{-6}

Table 1: Summary results and projected values of total error per gate, gate time durations for 1 qubit gate and 2 qubit gate for unprotected gate versus each respective PUDDING gate. Current ELSC (electronic grade single crystal from E6) sample is also compared to C^{12} enriched sample, which is expected to increase the coherence properties, allowing for lower EPG respectively.

V. DISCUSSION

A. Comparison with state-of-the-art

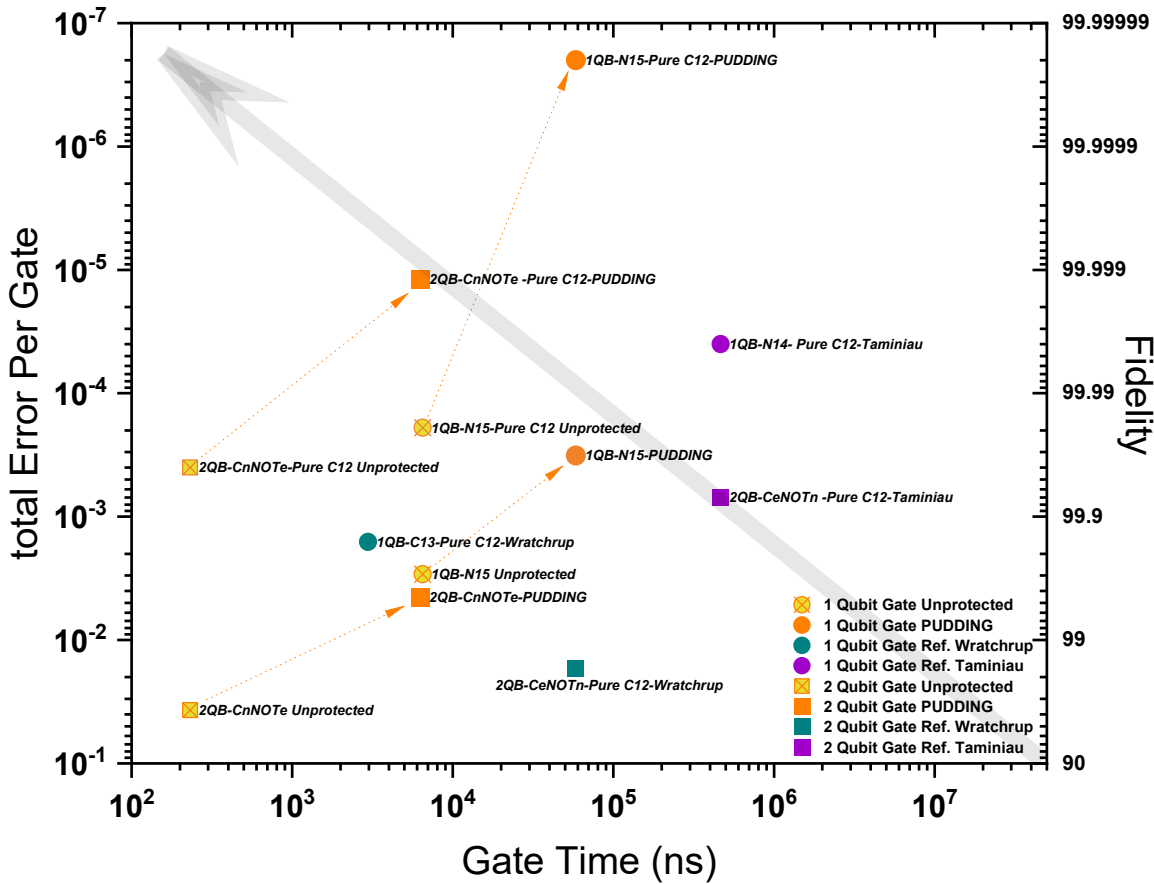


Figure 8: Error per gate versus gate time of state-of-the-art comparison of 1 and 2 Qubit performances achieved with NV [13,14].

Figure 8 reflects a comparison with earlier randomized-benchmarking studies on NV centers [13,14], which reported single-qubit rEPG $\sim 10^{-3}$ and two-qubit rEPG $\sim 10^{-2}$ without composite pulses, our work advances the state of the art through:

1. Systematic error decomposition, isolating RF power noise, electron relaxation, and dephasing.
2. First application of composite pulses to NV conditional gates, allowing from 9 to 27 \times improvement in error per gate.
3. Theoretical framework (PUDDINGS) generalizable to other platforms.

Our results can be compared with gate fidelities achieved in other leading platforms (Figure 9). Recent benchmarking in superconducting qubits has demonstrated single-qubit rEPG at or below 10^{-4} and two-qubit rEPG around 10^{-3} . Trapped-ion systems routinely achieve below- 10^{-4} errors for both single- and two-

qubit gates, albeit in ultra-high-vacuum and cryogenic environments. Neutral-atom platforms and semiconductor spin qubits are rapidly improving but still under active development.

In our room-temperature NV experiment with natural-abundance diamond, PUDDING-protected single-qubit gates achieve $EPG \simeq 2 \times 10^{-4}$, comparable to state-of-the-art superconducting-qubit performance, but in a solid-state defect platform operating at ambient conditions. Two-qubit PUDDING gates currently lag behind the best superconducting and ion-trap results. When projected to isotopically enriched ^{12}C diamond at 4 K, the PUDDING protocol approaches or surpasses the two-qubit error levels reported on any other platforms, while retaining the unique advantages of NV centers for integrated quantum networking.

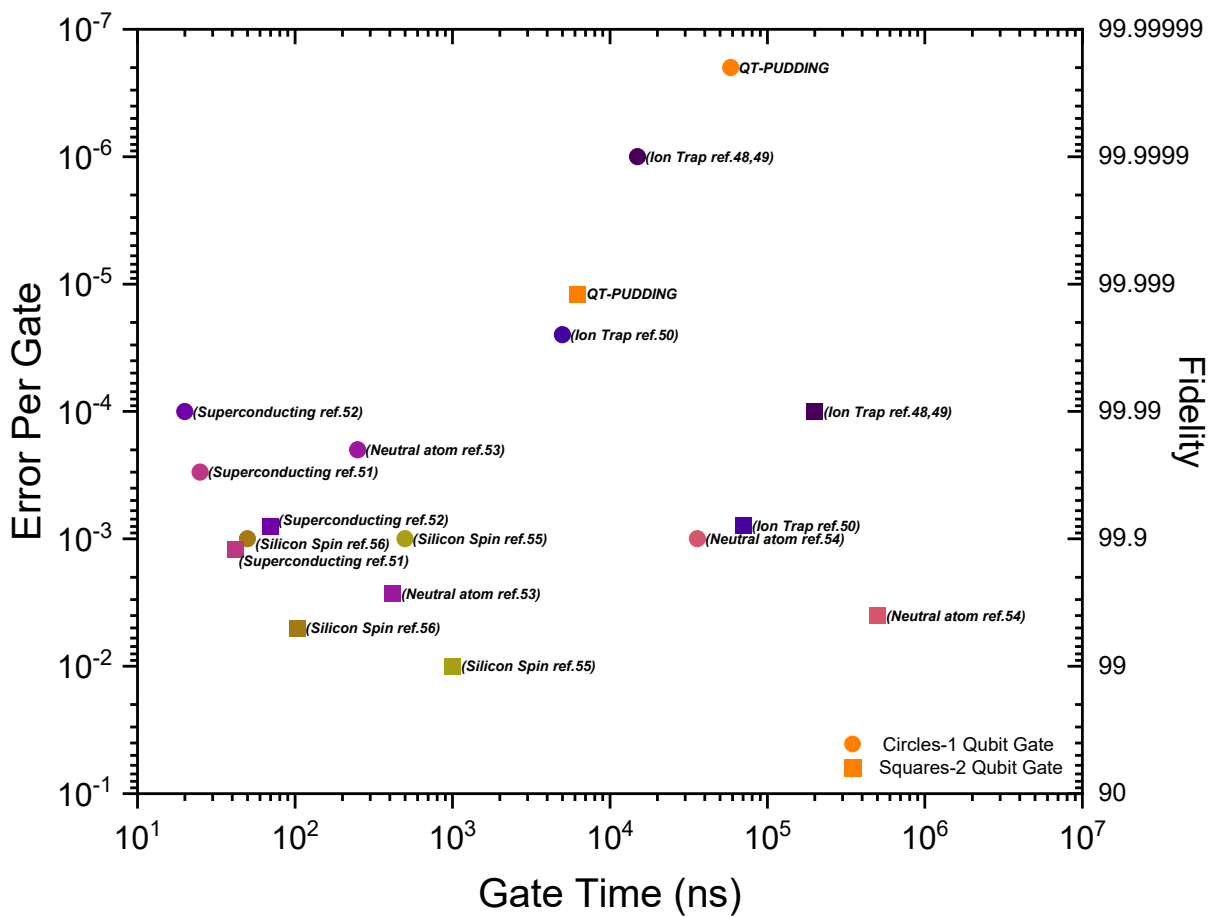


Figure 9: Comparison of single (circles) and two (squares) qubit gate error per gate (Fidelity) versus gate time performances of our actual applied PUDDING compared to current state-of-the-art performances achieved in different quantum computing modalities technologies [48], [49], [50], [51], [52], [53], [54], [55], [56].

B. Theoretical significance and generality of PUDDINGs

Beyond the specific NV implementation, the PUDDING construction addresses a broader theoretical question: can conditional gates be made intrinsically robust to both amplitude and detuning errors on both the identity and flip branches without sacrificing exactness? Our answer is yes, via a combination of zero-area structure, augmented symmetry, and composite embedding.

- (i) Zero-area structure ensures all-orders insensitivity to amplitude errors on the inactive subspace.
- (ii) Augmented symmetry in the form of P-ZAPs adds first-order detuning insensitivity on the resonant branch by enforcing time symmetry and additional constraints on the pulse components.
- (iii) Embedding P-ZAPs into broadband composite sequences extends this protection to the active branch, resulting in simultaneous first-order robustness against both amplitude and detuning errors throughout the conditional gate.

Because the only assumptions are a driven two-level system with a conditionally shifted transition frequency and the ability to shape amplitude and phase of the drive, PUDDINGs can be implemented in any architecture with energy-selective conditional interactions. This includes superconducting transmons with tunable couplers, exchange-coupled spins in semiconductor quantum dots, trapped ions with state-dependent AC Stark shifts, Rydberg-based neutral atoms, and rare-earth ion systems with hyperfine-coupled electron-nuclear pairs. The modular design also allows plug-and-play substitution of different BB-COMP backbones tailored to the dominant noise sources in a given platform.

VI. CONCLUSION

We have introduced and experimentally validated a comprehensive framework for error-protected quantum gates in NV centers in diamond, bridging theoretical pulse design with room-temperature randomized benchmarking. Our main achievements are: (i) experimental benchmarking of single- and two-qubit gates at room temperature, including a detailed error budget that isolates contributions from electron relaxation, dephasing, and control-power fluctuations; (ii) the development of PUDDINGs, a new class of composite conditional gates that combine protected zero-area pulses with broadband composite sequences to achieve first-order insensitivity to both amplitude and detuning errors on both active and inactive subspaces; and (iii) demonstration of substantial error suppression, with PUDDING-protected single-qubit gates achieving $EPG \simeq 2 \times 10^{-4}$ and two-qubit gates achieving $EPG \simeq 4 \times 10^{-4}$ – 5×10^{-3} at room temperature in natural-abundance diamond.

Using experimentally informed noise models, we project that in isotopically purified ^{12}C diamond operated at cryogenic temperatures, two-qubit PUDDING gates can achieve error per gate as low as 1.2×10^{-5} , more than two orders of magnitude below standard surface- and color-code thresholds. These results establish a new state-of-the-art benchmark, and demonstrate that NV centers can support gate fidelities competitive with leading superconducting [51], [52] and trapped-ion [48], [49], [50] platforms while offering unique advantages for quantum networking, including optical connectivity and long-lived nuclear memories.

More broadly, the convergence of precise pulse engineering, detailed noise modeling, and quantitative benchmarking realized here marks a significant step toward practical, distributed quantum computing. We

expect the ideas introduced in this work to inform the design of robust conditional gates across a wide variety of quantum technologies and to play a central role in the development of scalable, fault-tolerant quantum network architectures.

References

- [1] Y. Takada and K. Fujii, Improving Threshold for Fault-Tolerant Color-Code Quantum Computing by Flagged Weight Optimization, *PRX Quantum* **5**, 030352 (2024).
- [2] A. G. Fowler, M. Mariantoni, J. M. Martinis, and A. N. Cleland, Surface codes: Towards practical large-scale quantum computation, *Phys Rev A (Coll Park)* **86**, 032324 (2012).
- [3] A. M. Steane, Overhead and noise threshold of fault-tolerant quantum error correction, *Phys Rev A (Coll Park)* **68**, 42322 (2003).
- [4] N. Lacroix et al., Scaling and logic in the colour code on a superconducting quantum processor, *Nature* **645**, 614 (2025).
- [5] A. Hashim et al., Practical Introduction to Benchmarking and Characterization of Quantum Computers, *PRX Quantum* **6**, 030202 (2025).
- [6] J. Emerson, R. Alicki, and K. Zyczkowski, Scalable noise estimation with random unitary operators, *Journal of Optics B: Quantum and Semiclassical Optics* **7**, S347 (2005).
- [7] E. Knill, D. Leibfried, R. Reichle, J. Britton, R. B. Blakestad, J. D. Jost, C. Langer, R. Ozeri, S. Seidelin, and D. J. Wineland, Randomized benchmarking of quantum gates, *Phys Rev A (Coll Park)* **77**, 012307 (2008).
- [8] E. Magesan, J. M. Gambetta, and J. Emerson, Scalable and Robust Randomized Benchmarking of Quantum Processes, *Phys Rev Lett* **106**, 180504 (2011).
- [9] E. Magesan, J. M. Gambetta, and J. Emerson, Characterizing quantum gates via randomized benchmarking, *Phys Rev A (Coll Park)* **85**, 042311 (2012).
- [10] J. J. Wallman and S. T. Flammia, Randomized benchmarking with confidence, *New J Phys* **16**, 103032 (2014).
- [11] J. J. Wallman and S. T. Flammia, Corrigendum: Randomized benchmarking with confidence (2014 *New J. Phys.* 16 103032), *New J Phys* **18**, 079501 (2016).
- [12] G. Wolfowicz, F. J. Heremans, C. P. Anderson, S. Kanai, H. Seo, A. Gali, G. Galli, and D. D. Awschalom, Quantum guidelines for solid-state spin defects, *Nature Reviews Materials* **2021 6:10** **6**, 906 (2021).
- [13] T. Jaeger et al., Modeling Quantum Volume Using Randomized Benchmarking of Room-Temperature NV Center Quantum Registers, (2024).
- [14] H. P. Bartling et al., Universal high-fidelity quantum gates for spin qubits in diamond, *Phys Rev Appl* **23**, 034052 (2025).

- [15] H. Y. Carr and E. M. Purcell, Effects of Diffusion on Free Precession in Nuclear Magnetic Resonance Experiments, *Physical Review* **94**, 630 (1954).
- [16] S. Meiboom and D. Gill, Modified Spin-Echo Method for Measuring Nuclear Relaxation Times, *Review of Scientific Instruments* **29**, 688 (1958).
- [17] L. Viola and S. Lloyd, Dynamical suppression of decoherence in two-state quantum systems, *Phys Rev A (Coll Park)* **58**, 2733 (1998).
- [18] T. Gullion, D. B. Baker, and M. S. Conradi, New, compensated Carr-Purcell sequences, *Journal of Magnetic Resonance* (1969) **89**, 479 (1990).
- [19] J. Casanova, Z. Y. Wang, J. F. Haase, and M. B. Plenio, Robust dynamical decoupling sequences for individual-nuclear-spin addressing, *Phys Rev A (Coll Park)* **92**, 042304 (2015).
- [20] R. Tycko and A. Pines, Iterative schemes for broad-band and narrow-band population inversion in NMR, *Chem Phys Lett* **111**, 462 (1984).
- [21] M. H. Levitt, Composite pulses, *Prog Nucl Magn Reson Spectrosc* **18**, 61 (1986).
- [22] B. T. Torosov and N. V. Vitanov, Smooth composite pulses for high-fidelity quantum information processing, *Phys Rev A* **83**, (2011).
- [23] G. T. Genov and N. V. Vitanov, Dynamical suppression of unwanted transitions in multistate quantum systems, *Phys Rev Lett* **110**, (2013).
- [24] G. T. Genov, D. Schraft, T. Halfmann, and N. V. Vitanov, Correction of Arbitrary Field Errors in Population Inversion of Quantum Systems by Universal Composite Pulses, *Phys Rev Lett* **113**, 043001 (2014).
- [25] S. Wimperis, Iterative schemes for phase-distortionless composite 180° pulses, *Journal of Magnetic Resonance* (1969) **93**, 199 (1991).
- [26] S. Wimperis, Broadband, Narrowband, and Passband Composite Pulses for Use in Advanced NMR Experiments, *J Magn Reson A* **109**, 221 (1994).
- [27] J. T. Merrill and K. R. Brown, *Progress in Compensating Pulse Sequences for Quantum Computation*, in *Quantum Information and Computation for Chemistry* (2014), pp. 241–294.
- [28] H. K. Cummins and J. A. Jones, Use of composite rotations to correct systematic errors in NMR quantum computation, *New J Phys* **2**, 6 (2000).
- [29] B. T. Torosov, E. S. Kyoseva, and N. V. Vitanov, Composite pulses for ultrabroad-band and ultranarrow-band excitation, *Phys Rev A (Coll Park)* **92**, 33406 (2015).
- [30] K. Khodjasteh and L. Viola, Dynamically Error-Corrected Gates for Universal Quantum Computation, *Phys Rev Lett* **102**, 080501 (2009).

- [31] T. J. Green, J. Sastrawan, H. Uys, and M. J. Biercuk, Arbitrary quantum control of qubits in the presence of universal noise, *New J Phys* **15**, 095004 (2013).
- [32] L. Tsunaki, M. Dotan, K. Volkova, and B. Naydenov, Multi-Qubit Gates by Dynamical Decoupling Implemented with IBMQ and 15NV Center in Diamond, (2025).
- [33] M. C. Cambria et al., Temperature-Dependent Spin-Lattice Relaxation of the Nitrogen-Vacancy Spin Triplet in Diamond, *Phys Rev Lett* **130**, 256903 (2023).
- [34] M. H. Abobeih, J. Cramer, M. A. Bakker, N. Kalb, M. Markham, D. J. Twitchen, and T. H. Taminiau, One-second coherence for a single electron spin coupled to a multi-qubit nuclear-spin environment, *Nature Communications* 2018 **9**:1 **9**, 2552 (2018).
- [35] N. Bar-Gill, L. M. Pham, A. Jarmola, D. Budker, and R. L. Walsworth, Solid-state electronic spin coherence time approaching one second, *Nature Communications* 2013 **4**:1 **4**, 1743 (2013).
- [36] G. S. Vasilev and N. V Vitanov, Complete population transfer by a zero-area pulse, *Phys Rev A (Coll Park)* **73**, 23416 (2006).
- [37] M. W. Doherty, N. B. Manson, P. Delaney, F. Jelezko, J. Wrachtrup, and L. C. L. Hollenberg, The nitrogen-vacancy colour centre in diamond, *Phys Rep* **528**, 1 (2013).
- [38] A. M. Souza, G. A. Álvarez, and D. Suter, Robust dynamical decoupling, *Philosophical Transactions of the Royal Society A: Mathematical, Physical and Engineering Sciences* **370**, 4748 (2012).
- [39] W. Yang, Z.-Y. Wang, and R.-B. Liu, Preserving qubit coherence by dynamical decoupling, *Front Phys China* **6**, 2 (2011).
- [40] L. Viola, E. Knill, and S. Lloyd, Dynamical Decoupling of Open Quantum Systems, *Phys Rev Lett* **82**, 2417 (1999).
- [41] K. Khodjasteh and D. A. Lidar, Fault-Tolerant Quantum Dynamical Decoupling, *Phys Rev Lett* **95**, 180501 (2005).
- [42] I. Arrazola and J. Casanova, Robust oscillator-mediated phase gates driven by low-intensity pulses, *Communications Physics* 2023 **6**:1 **6**, 123 (2023).
- [43] C. H. Valahu, I. Apostolatos, S. Weidt, and W. K. Hensinger, Quantum control methods for robust entanglement of trapped ions, *Journal of Physics B: Atomic, Molecular and Optical Physics* **55**, 204003 (2022).
- [44] L. Dong, I. Arrazola, X. Chen, and J. Casanova, Phase-Adaptive Dynamical Decoupling Methods for Robust Spin-Spin Dynamics in Trapped Ions, *Phys Rev Appl* **15**, 34055 (2021).
- [45] A. J. Shaka and A. Pines, Symmetric phase-alternating composite pulses, *Journal of Magnetic Resonance* (1969) **71**, 495 (1987).

- [46] H. K. Cummins, G. Llewellyn, and J. A. Jones, Tackling systematic errors in quantum logic gates with composite rotations, *Phys Rev A (Coll Park)* **67**, 042308 (2003).
- [47] K. R. Brown, A. C. Wilson, Y. Colombe, C. Ospelkaus, A. M. Meier, E. Knill, D. Leibfried, and D. J. Wineland, Single-qubit-gate error below 10^{-4} in a trapped ion, *Phys Rev A* **84**, (2011).
- [48] A. C. Hughes, R. Srinivas, C. M. Löschner, H. M. Knaack, R. Matt, C. J. Ballance, M. Malinowski, T. P. Harty, and R. T. Sutherland, Trapped-ion two-qubit gates with $>99.99\%$ fidelity without ground-state cooling, (2025).
- [49] M. C. Smith, A. D. Leu, K. Miyanishi, M. F. Gely, and D. M. Lucas, Single-Qubit Gates with Errors at the 10^{-7} Level, *Phys Rev Lett* **134**, 230601 (2025).
- [50] M. Decross et al., Computational Power of Random Quantum Circuits in Arbitrary Geometries, *Phys Rev X* **15**, 021052 (2025).
- [51] R. Acharya et al., Quantum error correction below the surface code threshold, *Nature* **638**, 920 (2025).
- [52] M. AbuGhanem, IBM quantum computers: evolution, performance, and future directions, *J Supercomput* **81**, 687 (2025).
- [53] A. G. Radnaev et al., Universal Neutral-Atom Quantum Computer with Individual Optical Addressing and Nondestructive Readout, *PRX Quantum* **6**, 30334 (2025).
- [54] J. A. Muniz et al., High-Fidelity Universal Gates in the $\{171\} \mathbb{Yb}$ Ground-State Nuclear-Spin Qubit, *PRX Quantum* **6**, 20334 (2025).
- [55] M. T. Mądzik et al., Operating two exchange-only qubits in parallel, *Nature* **647**, 870 (2025).
- [56] T. Tanttu et al., Assessment of the errors of high-fidelity two-qubit gates in silicon quantum dots, *Nat Phys* **20**, 1804 (2024).

Appendix I: Functional dependence of error accumulation in various protocols for different noise channels.

Quantum Gate Protection Type:	Notation	Protected PUDDING -Gates		Non-Protected Gates		Dynamic Decoupling Protocols			Phase locked pulse bursts		
		2Qubit	1Qubit	2Qubit	1Qubit	CPMG	XY8	AXY	BB1	CORPSE	Narrowband Cphase
Protected operation		Cnot	full Clifford	Cnot	full Clifford	1&2Qubits			1Qubit gate		
Pulse frequency / detuning noise protection	ω	protected	protected	vulnerable	vulnerable	Identity			X		
Pulse Power / amplitude noise protection	p	protected	protected	sensitive	sensitive	protected	protected	Protected	sensitive	protected	sensitive
Systematic errors											
systematic detuning error	$\delta\omega$	$O(\delta\omega^2)$	$O(\delta\omega^2)$	$O(\delta\omega)$	$O(\delta\omega)$	$O(\delta\omega^2)$	$O(\delta\omega^2)$	$O(\delta\omega^2)$	$> O(\delta\omega)$	$O(\delta\omega^2)$	$\gg O(\delta\omega)$
systematic amplitude error	$\delta\alpha$	$O(\delta\alpha^2)$	$O(\delta\alpha^2)$	$O(\delta\alpha)$	$O(\delta\alpha)$	$> O(\delta\alpha)$	$O(\delta\alpha)$	$O(\delta\alpha^2)$	$O(\delta\alpha^2)$	$O(\delta\alpha)$	$> O(\delta\alpha)$
Frequent Calibration Requirement		not needed	not needed	Needed	Needed	Needed	Needed	Needed	Needed	Needed	Needed
Random errors											
random detuning error	T_2, T_2^*	$O\left(\left(\frac{1}{T_2}\right)^2\right) + O\left(\left(\frac{1}{T_2^*}\right)^2\right)$	$O\left(\left(\frac{1}{T_2}\right)^2\right) + O\left(\left(\frac{1}{T_2^*}\right)^2\right)$	$O\left(\frac{1}{T_2}\right) + O\left(\frac{1}{T_2^*}\right)$	$O\left(\frac{1}{T_2}\right) + O\left(\frac{1}{T_2^*}\right)$	$O\left(\frac{1}{T_2}\right) + O\left(\frac{1}{T_2^*}\right)$	$O\left(\frac{1}{T_2}\right) + O\left(\frac{1}{T_2^*}\right)$	$O\left(\frac{1}{T_2}\right) + O\left(\frac{1}{T_2^*}\right)$	$> O\left(\frac{1}{T_2}\right)$	$O\left(\frac{1}{T_2}\right) + O\left(\frac{1}{T_2^*}\right)$	$> O\left(\frac{1}{T_2}\right)$
random amplitude error	σ_α	$O(\sigma_\alpha^2)$	$O(\sigma_\alpha^2)$	$O(\sigma_\alpha)$	$O(\sigma_\alpha)$	$> O(\sigma_\alpha)$	$O(\sigma_\alpha)$	$O(\sigma_\alpha^2)$	$O(\sigma_\alpha^2)$	$O(\sigma_\alpha)$	$> O(\sigma_\alpha)$
Gate duration	$t_{\pi,elect}, t_{\pi,nuc}, \tau, \frac{1}{\Delta}$	$t_{PUDDING} = 6240\text{ns} \approx \frac{20}{\Delta}$	$(\sim 5t_{\pi,nuc}) \approx 58644\text{ns}$	$t_{\pi,nuc} = \frac{1}{\sqrt{2\Delta}} \approx 10t_{\pi,elect} = 232\text{ns}$	$t_{\pi,nuc} = \frac{1}{2} \approx 6.5\mu\text{s}$	$(< T_2)$	$1\mu\text{s} \leq 2N\tau \leq 50\mu\text{s}$	$1\mu\text{s} \leq 14\tau \leq 50\mu\text{s}$	$1\mu\text{s} \leq 14\tau \leq 50\mu\text{s}$	$\geq 3t_{\pi,elect} \approx 30 - 150\text{ns}$ or $\geq 3t_{\pi,nuc} \approx 30 - 300\mu\text{s}$	

The table presents the degree of protection of commonly-used schemes, as well as PUDDING, against various noise sources. The higher the power dependency in the error channel the better the protection. The systematic error channels are pulse amplitude (Rabi frequency) $\delta\alpha$ and detuning from resonance frequency $\delta\omega$. Good protection against systematic errors allows for longer working periods, without the need to frequently stop the system for calibrations. We acknowledge that systematic errors can in principle be calibrated out with the cost of system down time. Yet, improving the functional dependency in systematic error channels, can allow us to lessen the requirements of calibration (e.g. demanding infidelity of the order of 10^{-6} , requires calibrating the Rabi frequency only to $\frac{dp}{p} \approx 10^{-3}$ for a protocol with noise level of $O(dp^2)$). Random error channels are slow frequency detuning, drawn randomly from a Gaussian distribution of width $1/T_2^*$, at each application of the gate. T_2 is taken as the rate in which the frequency detuning changes during the gate application. The amplitude error is taken as a slow amplitude shift, constant over the application of each gate, drawn randomly from a Gaussian distribution of width σ_α . The duration of each gate is constructed depending on context from $t_{\pi,elect}$ is the fastest possible electron gate (typically 10-50 ns), $t_{\pi,nuc}$ is the fastest possible nuclear gate (typically 10-100 μs), τ is a delay which is in the order of the Larmor frequency time scale (typically 0.5-20 μs) and $\frac{1}{\Delta}$ is given by the energy difference between two resonances (typically 100-1000 ns).

Appendix II: Derivation of single qubit protected arbitrary gate

For the derivation of the parameters of a detuning- and amplitude-insensitive composite pulse of arbitrary rotation angle in single qubit, the rules of the game are:

We are given rotation matrices of two types. One type rotates by π , and the other rotates by some angle β . All the matrices rotate around an axis in the x-y plane. For each matrix, we are allowed to choose the phase, that is, the angle, ϕ , of the rotation axis from the x axis.

We are then asked to compose these matrices in such a way that the composite matrix would:

1. Rotate by a given angle, α about an axis in the x-y plane

2. Be unsensitive, to first order, to amplitude errors common to all the composing matrices.
3. Be unsensitive, to first order, to frequency errors common to all the composing matrices.

First, we have to determine the minimal number of matrices that are required. This can be done by counting the number of parameters needed to be set and the number of available conditions.

Let's assume that we take π matrices of n different phases (so we take at least $n \pi$ matrices, but can take more), and β matrices of m different phases (so we take at least m such matrices but can take more). Note that m cannot be zero, as then we would be limited to π or 2π rotations only, and we want to have an arbitrary overall rotation angle.

As a global phase does not matter, we thus have at most $m + n - 1$ phases to set. Further, we have to set β . So, in total, we'll have at most $m + n$ parameters to set.

How many conditions do we have? Any rotation matrix has three parameters in total. Of these, one parameter is left free (as we're not restricted to a specific angle in the x-y plane of the overall rotation axis), so this gives two conditions. Further, we want the first derivatives with respect to both amplitude and frequency deviations of all three parameters to be zero. This gives six additional conditions. Therefore, we have eight conditions in total. So, $m + n = 8$.

Now, if we work with time-symmetric sequences, the amplitude and frequency derivatives of two out of the three parameters of the composed matrix are automatically set to zero. This leaves only four conditions and therefore simplifies the problem considerably.

So, we now have $m + n = 4$. As the pulse sequence is symmetric, it will have to contain at least $2(m + n) - 1 = 7$ pulses. Without loss of generality, we choose $m = 1, n = 3$, and place the two β pulses at the beginning and the end of the sequence. This gives a sequence of the form $\beta_0 \pi_{\phi_1} \pi_{\phi_2} \pi_{\phi_3} \pi_{\phi_2} \pi_{\phi_1} \beta_0$, where, for example, π_{ϕ_1} indicates a π rotation about an x-y plane axis at an angle ϕ_1 from the x axis.

Having set the form of the sequence, finding the equations for the four conditions and solving them for the four parameters, β, ϕ_1, ϕ_2 , and ϕ_3 , reduces to a matter of some (rather lengthy but not too complicated) algebra. We obtain

$$\beta = \frac{\pi - \alpha}{2},$$

$$\phi_1 = g(\alpha),$$

$$\phi_2 = 2g(\alpha) + h(\alpha),$$

$$\phi_3 = 2g(\alpha) + 2h(\alpha),$$

with

$$g(\alpha) = \cos^{-1} \left(-\frac{\alpha}{4\pi} - \frac{1}{4} \cdot \sin \frac{\alpha}{2} \right),$$

$$h(\alpha) = \cos^{-1} \left(-\frac{\alpha}{4\pi} + \frac{1}{4} \cdot \sin \frac{\alpha}{2} \right).$$

Finally, having found the parameters of the rotation matrices, translating them into pulse parameters is straight forward. For example, for the most simple case of a constant Rabi frequency, Ω , the time durations of the pulses in the sequence would be simply π/Ω and β/Ω for the π and β matrices, respectively. The phase of each pulse would just be the rotation axis angle of the corresponding rotation matrix.

Appendix III: Conditions for detuning insensitivity near resonance

σ_x and σ_y : symmetric zero- π pulses

For a near-resonant pulse with a time-dependent, real Rabi frequency, $\Omega(t)$, and a fixed, small detuning, δ , the Hamiltonian is

$$H = \frac{\Omega(t)}{2} \sigma_x + \frac{\delta}{2} \sigma_z. \quad (6)$$

Performing a Magnus expansion up to second order in H , the propagation operator for the entire pulse (from $t = -\infty$ to $t = \infty$) is approximately

$$U \approx e^{M_1 + M_2}, \quad (7)$$

where,

$$M_1 = -i \int_{-\infty}^{\infty} H(t) dt, \quad (8)$$

$$M_2 = -\frac{1}{2} \int_{-\infty}^{\infty} dt \int_{-\infty}^t (H(t') H(t') - H(t') H(t)) dt'. \quad (9)$$

Inserting Eq. (6) into Eq. (8) and Eq. (9) we obtain

$$M_1 = \frac{i}{2} \sigma_x \int_{-\infty}^{\infty} \Omega(t) dt + \frac{i}{2} \sigma_z \delta T + O(\delta^2), \quad (10)$$

$$M_2 = \frac{i}{8} \delta \sigma_y \left(\int_{-\infty}^{\infty} t \Omega(t) dt - \int_{-\infty}^{\infty} \int_{-\infty}^t \Omega(t') dt' \right) + O(\delta^2), \quad (11)$$

where T is the pulse duration (for a finite-support pulse profile).

From Eq. (10) we see that for $\Omega(t)$ which area is zero (a zero π pulse), the σ_x component vanishes up to second order in δ .

From Eq. (11) we see that for $\Omega(t)$ which is both a zero- π pulse and is symmetric in time ($\Omega(-t) = \Omega(t)$), the σ_y component also becomes first-order insensitive to δ , as for this case both terms on the right hand side of Eq. (11) vanish. The first term vanishes as it is the first moment of an even function. The second term

vanishes as the integral of the Rabi frequency, which is even and starts at zero for $t = -\infty$, is an odd function, and thus its total area is also zero.

In a similar way, one can also show that for a symmetric zero- π pulse, all higher orders of the expansion contribute only σ_x and σ_y terms that are at least quadratic in δ .

However, from Eq. (10) we see that having a symmetric zero- π pulse is *not* a sufficient condition for the σ_z term to become first-order insensitive to δ , and thus additional conditions are required for complete first-order detuning protection.

σ_z : augmented pulses

We're given two pulses, A and C , of Rabi frequencies Ω_A and Ω_C and rotation angles α_A and α_C , respectively. Their transition matrices, up to first order in the detuning δ are

$$U_{A(C)} = \cos \frac{\alpha_{A(C)}}{2} I - i p_{A(C)} \sin \frac{\alpha_{A(C)}}{2} \sigma_x - i \sin \frac{\alpha_{A(C)}}{2} \frac{\delta}{|\Omega_{a(c)}|} \sigma_z, \quad (12)$$

where $p_{A(C)} = \text{sgn}(\Omega_{A(C)})$ is the sign of the Rabi frequency. The transition matrix of the combined pulse, CA , up to first order in δ is then

$$\begin{aligned} U_{CA} = & \cos \left(\frac{\alpha_A + p\alpha_C}{2} \right) I - i p_A \sin \left(\frac{\alpha_A + p\alpha_C}{2} \right) \sigma_x \\ & - i p \sin \frac{\alpha_A}{2} \sin \frac{\alpha_C}{2} \left(\frac{1}{\Omega_C} - \frac{1}{\Omega_A} \right) \delta \sigma_y \quad (13) \\ & - i \left(\frac{1}{|\Omega_A|} \sin \frac{\alpha_A}{2} \cos \frac{\alpha_C}{2} + \frac{1}{|\Omega_C|} \cos \frac{\alpha_A}{2} \sin \frac{\alpha_C}{2} \right) \delta \sigma_z, \end{aligned}$$

where $p = p_A p_C$ is the relative sign between Ω_C and Ω_A . We therefore see that the σ_z component of the combined pulse CA is insensitive to δ up to first order if

$$|\Omega_C| \tan \frac{\alpha_A}{2} = -|\Omega_A| \tan \frac{\alpha_C}{2}, \quad (14)$$

which proves Eq. (1). It is straight forward to see that the same condition applies also for AC .

To see that this condition is enough for the entire pulse to be first-order insensitive to the detuning, we note that under this condition, the pulse DB has the same transition matrix as that of CA , up to an opposite sign for the σ_x and σ_y components. This is as $\alpha_B = \alpha_A$, $\Omega_B = -\Omega_A$, and the relative sign between Ω_D and Ω_B is the same as that between Ω_C and Ω_A . Thus, for $DBCA$, these components will vanish, and it will have no first-order detuning dependency. In turn, this means the same for the full composite pulse $ACBDBCA$.

For the case that Eq. (1) does not hold, one can show using similar arguments that the transition matrix of the four component pulse $DBCA$ would read, up to first order in δ ,

$$U_{DBCA} = I - 2i\eta\delta \left[\sin \left(\frac{\alpha_A + p\alpha_C}{2} \right) \sigma_y + \cos \left(\frac{\alpha_A + p\alpha_C}{2} \right) \sigma_z \right], \quad (15)$$

with $\eta = \left(\frac{1}{|\Omega_A|} \sin \frac{\alpha_A}{2} \cos \frac{\alpha_C}{2} + \frac{1}{|\Omega_C|} \cos \frac{\alpha_A}{2} \sin \frac{\alpha_C}{2} \right)$. One can show that the transition matrix of the second part of the full pulse, U_{ACBD} would have the same structure, except for an opposite sign for the σ_y component. Thus, the full transition matrix would be of the form

$$U_{ACBDBAC} = I - 4i \cos \left(\frac{\alpha_A + p\alpha_C}{2} \right) \eta \delta \sigma_z + O(\delta^2). \quad (16)$$

This shows that in addition to the condition of Eq. (1), there is an alternative condition for first-order insensitivity of the full augmented symmetric zero-area pulse to δ ,

$$\cos \left(\frac{\alpha_A + p\alpha_C}{2} \right) = 0, \quad (17)$$

which proves Eq. (2).

Appendix IV Symmetric zero- π pulses of arbitrary conditional rotation angle

We consider an operation of the form,

$$U = U_+ U_- U_- U_+, \quad (18)$$

where

$$U_{\pm} = \cos \frac{\tilde{\alpha}}{2} I - i \sin \frac{\tilde{\alpha}}{2} (\pm \sin \beta \sigma_x + \cos \beta \sigma_z). \quad (19)$$

Here

$$\tan \beta = \frac{\Omega}{\Delta}, \quad (20)$$

where Ω is the Rabi frequency and Δ is the detuning of the off-resonant transition, and $\tilde{\alpha}$ is the rotation angle of the detuned transition. The rotation angle of the resonant transition, α , is related to $\tilde{\alpha}$ by

$$\alpha = \tilde{\alpha} \cdot \cos \beta. \quad (21)$$

This form of U ensures that the total pulse area vanishes and that the pulse sequence is time-symmetric. While it is not the most general form to do so, it is one of the simplest, as it requires only a single amplitude value for all the components.

As we have two parameters to set, $\tilde{\alpha}$ and β , we need two requirements. The first is that the total rotation induced by U for the detuning Δ has no z component, such that for the detuned transition, U acts as if it was a simple, resonant pulse. Thus, the coefficient of σ_z within U must vanish. One can show that this leads to the equation

$$\cos \tilde{\alpha} \cos^2 \beta + \sin^2 \beta = 0. \quad (22)$$

The second requirement is that the overall rotation angle induced by U for the detuned transition has a specified value, θ . This means that the coefficient of the I component of U is $\cos(\theta/2)$. This leads to the equation

$$\cos 2\tilde{\alpha} \cos^2 \beta + \sin^2 \beta = -\cos \frac{\theta}{2}. \quad (23)$$

One can then reach an equation for $\tilde{\alpha}$,

$$\cos \tilde{\alpha} (\cos 2\tilde{\alpha} - 1) = (\cos \tilde{\alpha} - 1) \left(\cos 2\tilde{\alpha} + \cos \frac{\theta}{2} \right). \quad (24)$$

Expanding $\cos 2\tilde{\alpha}$ in terms of $\cos \tilde{\alpha}$, dividing both sides by $\cos \tilde{\alpha} - 1$ ($\tilde{\alpha} \neq 0$), and rearranging, we arrive at

$$\cos \tilde{\alpha} = -\sin^2 \frac{\theta}{4}. \quad (25)$$

Plugging this into Eq. (14) then yields

$$\tan \beta = \sin \frac{\theta}{4}, \quad (26)$$

which together with Eq. (20) gives Eq. (4).

Finally, using Eq. (21) we obtain

$$\alpha = \cos \beta \cos^{-1} \left(-\sin^2 \frac{\theta}{4} \right), \quad (27)$$

which together with Eq. (26) gives Eq. (5).

Appendix V Simulation of dynamical noise

In order to add a finite homogeneous dephasing time to our model, we introduce a random, time-varying detuning, $\delta(t)$, to the Hamiltonian and solve for the propagation matrix numerically. We take the frequency content of $\delta(t)$ to be given by a truncated $1/f$ distribution. For this we set

$$\delta(t) = \frac{A}{T_2^*} \sum_{n=1}^N \frac{1}{n} \cos \left(\frac{2\pi f_c}{N} nt + \phi_n \right), \quad (28)$$

where ϕ_n is a random number drawn from a uniform distribution between 0 and 2π , f_c is the cutoff frequency, N is fixed number much larger than 1 (we take $N = 100$), T_2^* is the inhomogeneous dephasing time, and A is a dimensionless constant.

We first set $1/f_c \gg T_2^*$ and fix A such that the decay time of a simulated Ramsay experiment is T_2^* . Then, for each value of T_2^* , we set f_c such that the decay time of a simulated Hahn echo experiment is T_2 .

We repeat the calculation for fifty realizations of $\delta(t)$. For each realization we calculate the mean of the squares of the differences between the elements of the obtained matrix and the ideal matrix and take the overall fidelity to be the square root of the mean of all of these values.

Appendix VI: Randomized Benchmarking experiment procedure

Randomized benchmarking of single-qubit gates. The system is initialized in the state $|1_e\rangle \otimes |0_N\rangle$. N random Clifford operations are then applied on the nuclear spin, followed by the inverse gate sequence, ideally returning to the initial state. The probability of returning to the initial state is measured and plotted against the number of gates. $|1_e\rangle \otimes |0_N\rangle$. Then we applied MW pulses that corresponds to $IC_N not_e = |I_e\rangle\langle I_e| \otimes |1_N\rangle\langle 1_N| + |X_e\rangle\langle X_e| \otimes |0_N\rangle\langle 0_N|$ ending in $|0_e\rangle \otimes |0_N\rangle$ and measuring with green laser $|0_e\rangle\langle 0_e|$. Each member of the Clifford group is done by applying $Z_{\phi_1}X_{\phi_2}Z_{\phi_3}$ rotations of the nuclei. The Z rotations are done by phase jump in our clock. And the X rotations are either π or $\frac{\pi}{2}$ rotations. The data is fitted to $P(N) = Ae^{-B \cdot N} + C$, extracting the average error per gate as $EPG = \frac{1-e^{-B}}{2}$. For the reference data, the same initialization and measure protocols were used, where instead of applying the gates, the system was kept idle for the same duration as that of the gates.

Benchmarking of a two-qubit gate. The system is initialized in the state $|0_e\rangle \otimes |1_N\rangle$. N $C_n NOT_e$ operations are then applied, followed by the inverse gate sequence, ideally returning to the initial state. The probability of returning to the initial state is measured and plotted against the number of gates. The data is fitted to $P(N) = Ae^{-B \cdot N} + C$, extracting the average error per gate as $EPG = \frac{1-e^{-B}}{2}$.

Appendix VII:

Diamond Sample Purity Grade	Temperature:	300K	4K
ELSC	Electron spin		
	T1 (sec)	5.7x10 ⁻³	>> 60
	T2(sec)	4x10 ⁻⁵	4x10 ⁻⁵
	T2*(sec)	2.99x10 ⁻⁶	2.99x10 ⁻⁶
	Nuclear Spin		
	T1(sec)		>>60
	T2(sec)		
	T2*(sec)	3.21x10 ⁻³	7.35x10 ⁻³
C ¹²	Electron spin		
	T1(sec)	2.22ms	>>60
	T2(sec)	429us	1.8x10 ⁻³
	T2*(sec)	12.85us	3x10 ⁻⁴
	Nuclear Spin		
	T1(sec)	100s	>>60
	T2(sec)	3.33ms	5.7s / 8s*
	T2*(sec)		550ms /170ms**

Table 2: Coherence time properties summary [33], [34], [35]